Study of Modified Optical Properties of $TiO_2/Au/TiO_2$ multilayered thin films by chemical vapor deposition

By

Muhammad Hasan

School of Chemical and Materials Engineering

National University of Sciences and Technology

2022

Study of Modified Optical Properties of $TiO_2/Au/TiO_2$ multilayered thin films by chemical vapor deposition

Name: Muhammad Hasan

Reg. No: 00000277548

This thesis is submitted as a partial fulfillment of the requirements for the degree of

MS in Nanotechnology and Engineering

Supervisor Name: Dr. Muhammad Shoaib

School of Chemical and Materials Engineering (SCME)

National University of Sciences and Technology (NUST),

H-12 Islamabad, Pakistan.

July, 2022

Dedication

With deep sense of gratitude, humbleness, and warmest affection I would like to dedicate this thesis to my family and colleagues for their continuous help and support.

Acknowledgment

All gratitude and praises are to **Allah Almighty**, the most gracious and the most merciful. He is the entire source of knowledge to mankind. He blessed us with health, thoughts, and helped me achieve this goal. After Almighty Allah, praises are for Prophet Muhammad (S. A.W.), the most perfect and exalted human being who provided us guidance and knowledge.

I would like to express sincere gratitude to my supervisor Dr. Muhammad Shoaib and co-supervisor Prof. Dr. Arshad Saleem Bhatti, Rector of Virtual University who accepted me as a postgraduate student and provided me a chance to work with them. I am truly very fortunate to have the opportunity to work under their supervision and grateful for my advisement, guidance, and support throughout my work. The professional research skill and personal lessons that I have learned from them are invaluable for future endeavors. Also, I am very grateful to all my teachers who helped me and motivated me to do my best.

I am greatly indebted to all my colleagues in CMND, COMSATS who have graciously applied themselves to the task of helping me with support and valuable suggestions. A special thanks to Dr. Fahad Bhopal and all the other senior research students for their help and support. I pay my regards to my colleagues especially Umer Ijaz, Ibtisam Ahmed and Mazhar Tanveer for their help and guidance in my work.

Finally, I am thankful to my family, especially my great mother for supporting me through thick and thin and for being there for me throughout my life endeavors.

Muhammad Hasan

Reg. No.: 00000277548

Abstract

Wide band gap semiconductors have efficient UV absorption and very low absorption in the visible spectrum. The surface plasmon resonance (SPR) phenomenon of gold is used to change the optical properties of TiO_2 in this study. In this study metal sandwiched planar (TiO_2/Au/TiO_2) structures were studied using a variety of optical techniques, including spectroscopic ellipsometry, UV/Vis absorption, and photoluminescence spectroscopy (PL). UV/Vis spectroscopy of TiO_2/Au/TiO_2 unfolded the presence of two broad bands in the visible range that were not present in TiO_2 thin film. This was attributed to improved interband and plasmon resonance oscillations of Au in a dielectric environment. Photoluminescence spectroscopy revealed three types of luminescent centers in TiO_2 around 351nm, 520nm and in the IR range. PL also revealed the introduction of near band gap edge defects as well as a rounded peak in composite films. UV/Vis spectroscopy revealed enhanced absorption in the visible region for composite films compared to a simple absorption spectrum for TiO_2 only. 1nm thickness showed a drastic amount of absorption intensity compared to any other thickness. With the increase in the thickness of gold, this absorption intensity can be observed to be decreasing. In composite films with thickness of Au to be 5nm, 10nm and 20nm surface plasmon resonance modes are observed around 730nm, 670nm and 620nm respectively showing a shift in SPR modes towards smaller wavelength.

Table of Contents

List of Figures

List of Tables

Chapter - 1

1 Introduction

1.1 Nanoscience and Nanotechnology

The word ‘Nano’ originated from the Greek word ‘dwarf’. Nanoscience deals with the study of manipulating material at the molecular and atomic scale to achieve different properties than those at bulk. Nanotechnology is the art of controlling dimensions at nanometer scale and ultimately designing, characterizing, and applying those materials in various aspects of life. If 1 meter is divided into one billion equal pieces then one of those pieces equals the size of 1 nanometer. An inch is made up of 25,400,000nms. The thickness of a sheet of newspaper is around 100,000 nm [1].

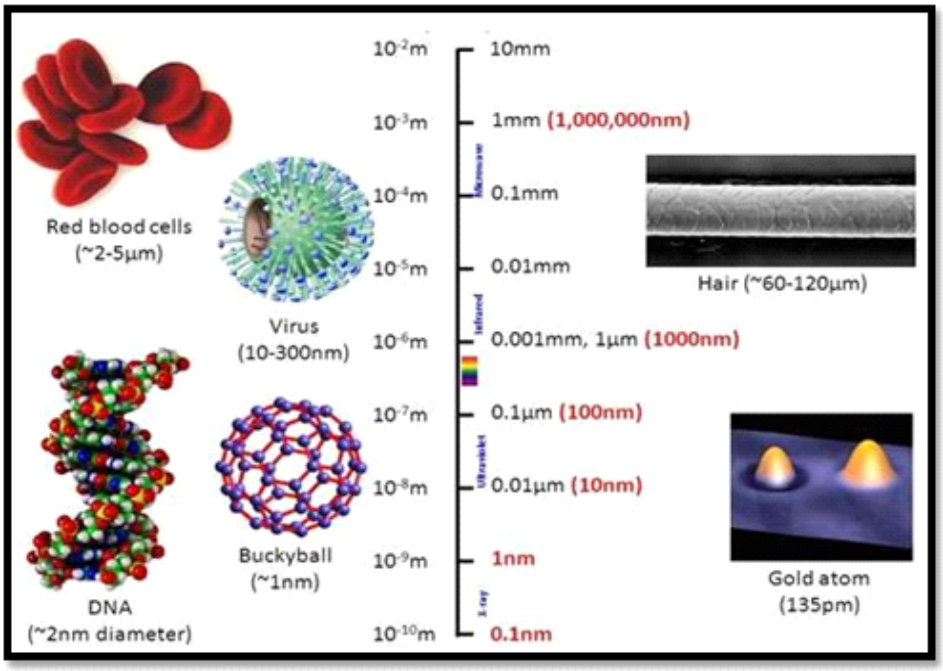

Figure 1.1: Objects at Nanoscale.

A well-renowned Physicist Richard Feynman in his famous talk entitled “There is Plenty of Room at the Bottom” on December 29, 1959 [2] proposed the concept that scientists will be able to modify and control individual atoms and molecules.

1.2 Applications of Nanoscience and Nanotechnology

Nanoscience and Nanotechnology have their applications in major science fields like Physics, Material Sciences, Chemistry, Biology and semiconductor physics, etc. Nanotechnology can produce numerous modern equipment and gadgets with tremendous applications in pharmaceutical, biotechnology, and energy storage such as microchips, flexible touchscreens, sunscreens and for the treatment of cancer [3].

1.3 Dimensional Classification of Materials

Nanomaterials can be classified dimensionally based on nanostructure elements present in that material having dimensions as three, two, one and zero. The dimensional classification shows the degrees of freedom in particle momentum. The relation amid the density of states and the energy of materials in different dimensions is shown in figure 1.1. The density of state changes significantly as we move from bulk to zero-dimensional material as the degree of confinement also varies with the dimension of a material. Examples of nanostructures in different dimensions are demonstrated in figure 1.2.

1.3.1 Zero Dimension

In 0-D, the motion of electrons is confined in every direction. Examples are quantum dots, nanoclusters etc.

1.3.2 One Dimension

In 1-D, electrons can move freely in a single direction; the motion is restrained in the remaining two directions. Examples are nanorods and nanowires etc.

1.3.3 Two Dimension

In 2-D, electrons can move freely in two directions; the motion is restrained in a single direction. Examples are branched structures and nanofilms etc.

1.3.4 Three Dimension

In 3-D, electrons are able to move freely in all possible directions. Examples are powders, polycrystalline materials, etc.

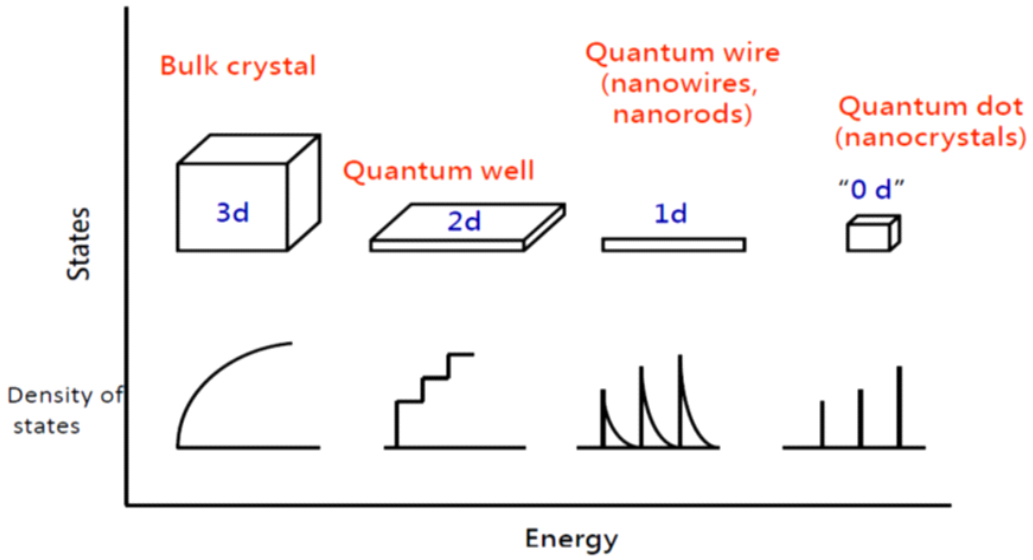

Figure 1.2: 0-D, 1-D, 2-D, 3-D materials and their density of states

1.4 Energy Sources

Scientists are continuously in search of efficient energy sources to meet modern day world energy requirements. Most of the energy available is nonrenewable because of limited supplies. These energy sources include petroleum, hydrocarbon gas liquids, natural gas, coal and nuclear energy. However, there are 5 major renewable energy sources which are solar energy, geothermal energy, wind energy, biomass and hydropower [4].

These sources are naturally replenished hence they are easily available. Solar energy attracts the interest because it is available every day in almost all countries of the world however cost associated with solar technology is a limiting factor. For the conversion of sunlight, photovoltaic devices absorb solar energy and convert it into electrical energy.

Nanomaterials play a great role in the efficiency enhancement of photovoltaic devices. These photovoltaic devices are divided into three generations. 1st generation of PV devices consists of solar cells with a single junction that is created with pure silicon biscuits. The efficiency achieved by first generation of solar cells is 25% and η is inadequate at about 30% [5]. While enhancing the material as well as the processing cost of generating such PV technologies led to its second generation. The greatest effective technologies in second generation were copper indium gallium (di) selenide (CIGS), amorphous Si and Cadmium telluride (CdTe). For lab-scale devices, this generation achieved the highest recorded efficiency at 19% and for commercial module, 14% efficiency was recorded. 3rd generation of photovoltaic generations uses thin films and deposition methods of second generation alongside using approaches such as multiple energy level approach, tandem solar cells, concentrator systems, multiple carrier excitation and up/down conversion. This improved the efficiency as well as lowered the overall cost of solar cells however research in this area is in its early stage [6].

1.5 Surface Plasmon Resonance

A localized electric field is created around metallic nanostructures by the collective flow of electrons. The concentrated electric field causes greater trapping/scattering of incoming photons, which can change the host/surrounding material's optical/electrical characteristics to Au NPs. The enhanced light localization/scattering effects caused by Au electron surface plasmon resonance effects have been widely researched. Both SPR effects of Au nanoparticles and interband transitions can be used to alter the optical properties of a semiconductor [7].

Surface plasmons are oscillating electron waves that confine an electromagnetic field with a higher intensity than the incident field at metallic surfaces. When a plasmon is struck by an external field, its oscillations reach their peak at a frequency called plasmon resonant frequency. At a resonant frequency, maximum absorptions are seen. The resonant phenomena of metallic surfaces is now employed in a broad array of applications such as biomedical, optical sensors, energy harvesting and storage devices. The size and form of the metallic NPs, and composition of the surrounding dielectric medium, all influence the resonance frequency of oscillating electrons [8]. The

absorption peak red moves from 510 to 580 nm when the size of the gold nanoparticles changes from 13nm to 90 nm. Charge carriers are highly separated at the borders of smaller nanoparticles, and different dipole moments produce absorptions at elevated energies. Higher order multipolar terms arise as the size of the nanoparticle grows, resulting in less absorption and more scattering. It demonstrates that in TiO_2, absorption occurs exclusively at direct band gap permitted transitions. Absorption in Au NPs is detected at 522 nm, which is the SPR frequency. The total optical characteristics of the combined metal/semiconductor hybrid structure are defined by the superposition of the two wave functions (excitonic and plasmonic).

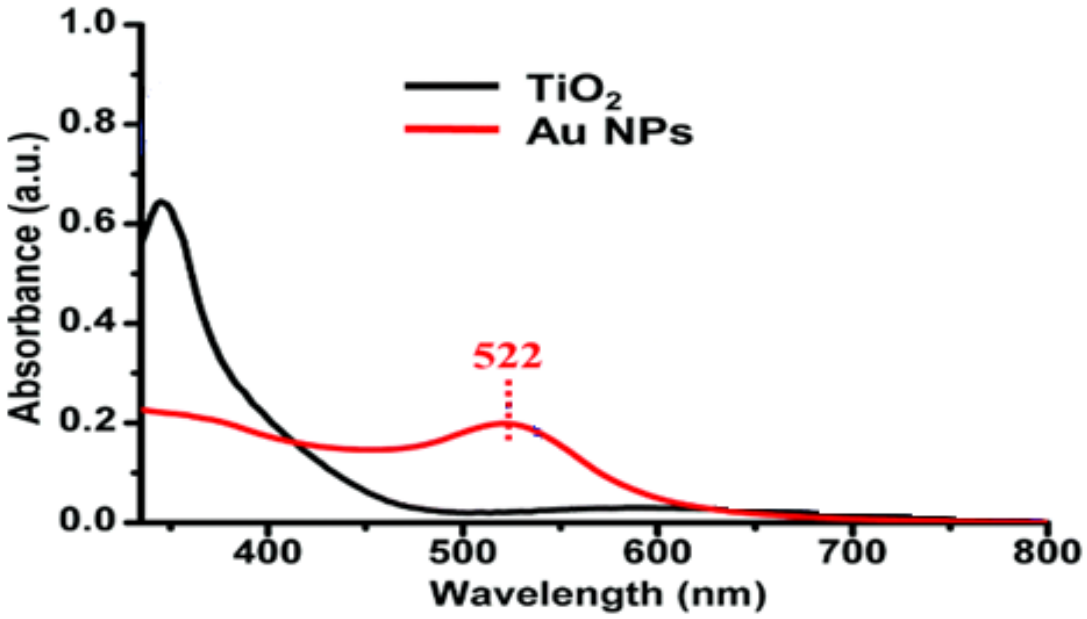

Figure 1.3: Absorption spectra for TiO_2 thin films and Au NPs [9]

A localized electric field is created around metallic nanostructures by the collective flow of electrons. The concentrated electric field causes greater trapping/scattering of incoming photons, which can change the host/surrounding material's optical/electrical characteristics to Au NPs. The enhanced light localization/scattering effects caused by Au electron surface plasmon resonance effects have been widely researched. Both SPR effects of Au nanoparticles and transitions within bands can be used to modify the optical properties of a semiconductor.

1.6 Scope of Present Work

In this thesis, TiO_2 and gold nanoparticles are deposited by chemical vapor deposition. The thickness of TiO_2 is kept constant while the thickness of Au layer is varied in each sample. This will help us to study the SPR effect of Au layer placed between TiO_2 layers and effect of different thicknesses of gold on optical properties such as energy harvesting, etc.

Chapter 2

2. Literature Review

2.1 Titanium Dioxide

Titanium Dioxide is a powder of white color. It has no odor and exists in 3 crystalline forms: anatase, brookite and rutile. It possesses the chemical formula of TiO_2. It occurs naturally as an oxide of Ti [10]. It is found in condensers, paints, painting colors, plastics, printing ink, paper, rubber, ceramics, crayons and electronic components [11].

Figure 2.1: TiO_2 Nanoparticles (20nm) [12].

Hydrothermal procedures, sol-gel synthesis, microwave techniques and green chemistry etc. are other ways used to make synthetic TiO_2 [13,14]. By carefully designing and modifying the process parameters, it is possible to acquire the required materials with modified specific physicochemical properties, such as surface area, nanoparticle morphology and form, nanoparticle size and uniformity in size, crystallinity and crystal phase, photoactivity, and many others by substrates used, ratio of solvents, temperature and processing time. These characteristics can also be altered during the synthesis of

NPs by adding different surfactants, dopants, or by post-synthesis changes such as doping, surface functionalization, or organic molecule binding [15, 16]. Titanium-dioxide nanoparticles' widespread use is due to their low toxicity and this property can be altered by combining them along with photosensitizers [17].

Table 2.1: Physical properties of Titanium Dioxide [18, 19, 20, 21, 22].

Physical Properties	**Unit**	**Crystalline Silica**
Melting point	Degree Celsius	Approx. 1843
Boiling point	Degree Celsius	Approx. 2972
Density	g/cm^3	4.23
Refractive Index	--	2.61
Specific resistivity	W/cm	$> 10^{13}$
Thermal Conductivity (Bulk TiO_2)	$Wm^{-1}K$	8.5
Poisson's Ratio	-	0.27

2.1.1 Structure of Titanium Dioxide

Titanium (IV) dioxide is mostly created by purifying rutile or exposing ilmenite ($FeTiO_3$) to chloride or sulfate procedures, which result in pure TiO_2. Calcination takes place at roughly 400 C, can change amorphous TiO_2 into anatase or brookite when heat treatment is performed. When temperature reaches above 600 °C, these polymorphs are transformed to rutile [15,23,24]. The crystal structure of TiO_2 is closely linked to its

unique qualities, which are also linked to its manufacturing technique. Anatase, rutile, and brookite are the three crystal formations of TiO_2 [25] which can be seen in figure 2.2.

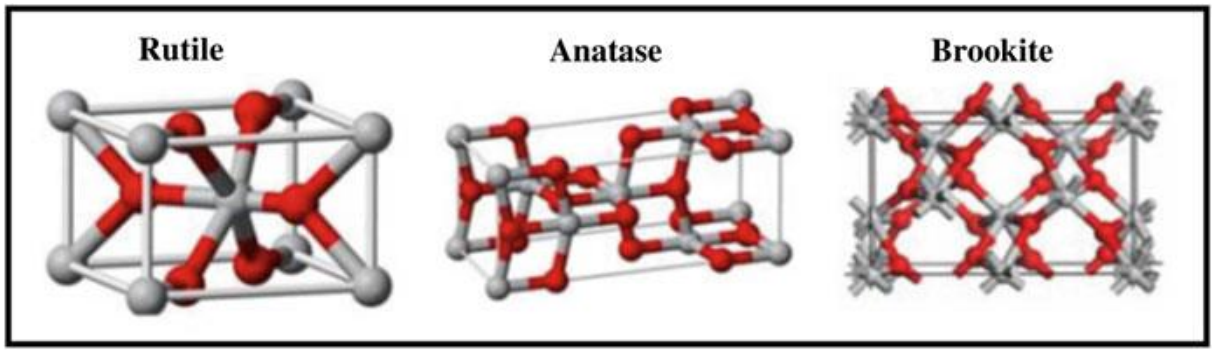

Figure 2.2: Different structures of TiO_2

2.1.2 Properties of Titanium Dioxide

Following are the properties of TiO_2 nanoparticles.

Titanium (Ti), the earth's tenth most prevalent element, is highly spread. Ti has an average content of 4400 mg/kg in the earth's crust. Ti does not occur in the metallic state in nature due to its high affinity for oxygen and other elements. The most frequent oxidation state of Ti is +4, though there are also +3 and +2 states. The most often utilized compounds in the industry are metallic Ti, TiO_2 and TiCl4.

TiO_2 (CAS: 13463-67-7) is the naturally occurring oxide of titanium, commonly known as titanium (IV) oxide, titanic acid anhydride, titania, titanic anhydride, or Ti white. It has a molecular weight of 79.9 g/mol. It has a melting point of 1843°C, a boiling point of 2972°C and a relative density of 4.26 g/cm3 at 25°C. TiO_2 is a water-insoluble particle.

Among anatase and rutile, the two crystal forms of TiO_2, anatase is more chemically reactive [26,27]. TiO_2 rutile has a lesser toxic potential than anatase [28,29].

In most cases, TiO_2 nanoparticles are a combination of rutile and anatase crystal forms. Shape, size, surface features, and interior structure are the most important elements impacting particle physicochemical attributes. Chemically, TiO_2 FPs (the rutile form)

are thought to be non-reactive. However, when the particle size decreases, the surface area of the particles increases [30]. TiO_2 is entirely insoluble in water, dilute acids, or general organic solvents. It may be dissolved at high temperatures in concentrated sulfuric or hydrofluoric acids [31].

Because of its high dielectric constant, titanium dioxide has excellent electrical characteristics. It is a non-toxic and stable compound. Oxygen, hydrogen sulphide, sulphur dioxide, carbon dioxide, and ammonia do not react with it. In the event of extended boiling, it may react with sulfuric acid and hydrofluoric acid [32]. As a result, TiO_2 in the form of anatase has a greater photoactivity than TiO_2 in other forms.

The gaps produced in the valence bands of both anatase and rutile have a high oxidation power because the valence band energies of both anatase and rutile are very low. The anatase shows n-type semi conductivity due to the band gap energies, whereas rutile is an unstable p-type semiconductor.

2.1.3 Titanium Dioxide Applications

Great efforts in research regarding TiO_2 have proved fruitful in providing many applications in environmental and energy related areas of the world [33]. These include areas varying from sensors and photo-electrochromics to photocatalysis and photovoltaics. [34].

Figure 2.3 indicates a few of the many applications of titanium dioxide.

Figure 2.3: Applications of TiO_2 [33]

2.2 Gold

Gold is a transition metal. It is part of group 11 period 6 and is found in block D of the periodic table and has atomic number 79. Gold nanoparticles often exist in colloidal form. In its pure form, it is found in slightly reddish yellow color. It is a nanoparticle solution in water or any other fluid. It has optical properties that help strongly reflect yellow and red thus transmitting greenish blue light. For spherical particles smaller than 100 nm, it is frequently bright red, while for bigger spherical particles, it is blue/purple.

It is a good conductor of electricity and heat. Gold nanoparticles exhibit unique optical properties including two famous features which are surface plasmon resonance and the color change upon aggregation [35,36,37]. Au nanomaterials can be created with different morphologies and structures such as nanospheres, nanorods, nanoshells and nanocages et cetera [38].

Characteristics of Au nanoparticles rely on shape and size. Its strength increases when it is alloyed continuously. It is a strong conductor of heat as well as electricity [39]. When chemically inert, it serves as a good infrared reflector. Gold nanoparticles are frequently covered with small molecules, polymers, and biological recognition molecules because of their versatile surface chemistry.

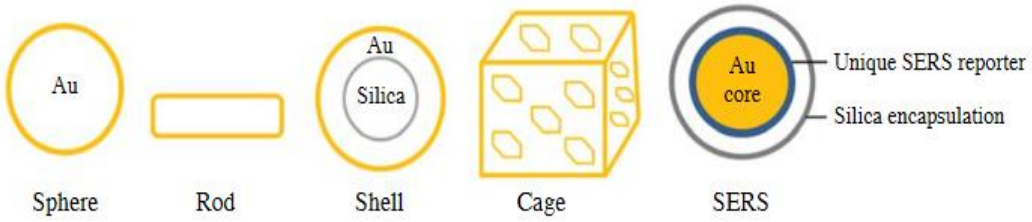

Figure 2.4: Schematic representation of various Au nanomaterials [38]

2.2.1 Structure of Gold

Colloidal gold is a solution containing gold nanoparticles suspended in a fluid, most often water. It is frequently red, blue, or purple in color, depending upon the size of the spherical particles smaller than 100nm. The characteristics of colloidal gold nanoparticles are mostly determined by their size and form.

2.2.2 Properties of Gold Nanoparticles

The physical properties of Au NPs are highly impacted due to their size because gold nanoparticles' electronic structure changes with shape and size. Large band gaps can be found in small gold clusters. The surface plasmon resonance (SPR), which gives colloidal solutions of spherical Au NPs their typical bright red appearance, is the most prominent optical feature of Au NPs with sizes varying from 2 to 100 nm. Au NPs with a size greater than 2 nm have bigger extinction cross-sections than other organic and inorganic chromophores, allowing for 100 percent light-to-heat conversion efficiency, strong photostability, and the capacity to increase the electromagnetic field near the surface of metal. Smaller clusters, on the other hand, have well-defined and unique absorption properties.

The wavelength of surface plasmon resonance is proportional to particle size; hence, as particle size increases, the wavelength becomes redder and longer. Red light is absorbed, while blue light is reflected, resulting in pale blue or purple color solutions [40,41]. Physical properties of gold can be seen in table 2.2.

Table 2.2: Physical properties of gold.

Physical properties	**Metric**	**Imperial**
Density	19.30 g/cm^3	0.697 lb/in^3
Molar mass	196.97 g/mol	-
Melting point	1064.43^{o}C	1947.9741^{o}F
Boiling point	2807^{o}C	5084.6^{o}F

With the increase in particle size, the SPR wavelengths move into the infrared region of the electromagnetic spectrum. These wavelengths are transparent, giving NPs a translucent or clear color. SPR may be influenced by changing the size or form of the nanoparticles.

Figure 2.5: Colors of various sized monodispersed gold nanoparticles [42].

Because of the flexibility of gold particles' surface chemistry, they may be coated with a variety of components such as biological recognition molecules, polymers, and tiny molecules. As a result, gold nanoparticles are now used in medicinal, chemical, as well as for optical applications.

2.2.3 Applications of Gold Nanoparticles

There is a massive flow of new Au NP applications with each passing day. Gold nanoparticles offer unique physical and optical properties involving surface plasmon oscillations which have applications in sensing, imaging and labeling. Owing to better biocompatibility, they are a great source of the biosensor as well as biomedical applications in therapeutics and disease diagnosis [38]. These nanoparticles can also connect electronic chip components, conductors and resistors and this makes them an integral part of chip designing.

Au nanostructures can be used in the detection of various molecules using Surface Enhanced Raman scattering (SERS) due to SERS's high sensitivity and selectivity. Local surface plasmon resonance (LSPR) of Au nanostructures is sensitive to local dielectric constant of the surrounding environment ultimately making them a good choice for refractive index sensing [43]. Many other applications of gold nanoparticles are shown in figure 2.6.

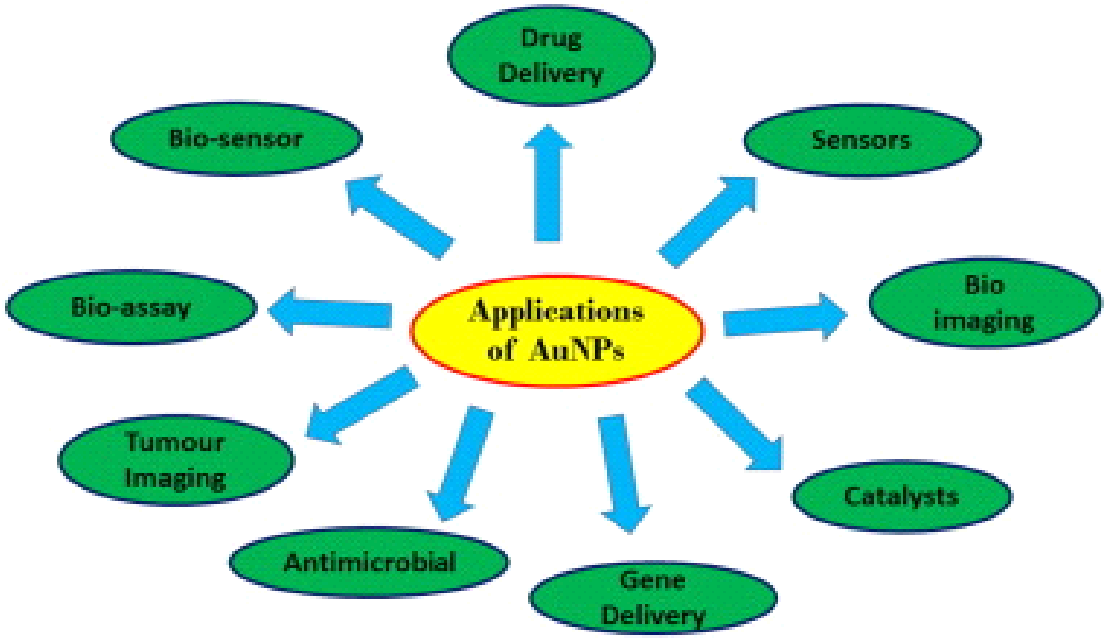

Figure 2.6: Applications of gold nanoparticles [44]

2.3 Synthesis Techniques of Metal Nanoparticles

There are many techniques used to make metallic nanoparticles. Some of them are explained below.

2.3.1 Spin Coating

Spin coating synthesis is used for creating smooth thin coatings on substrates. The coating material is placed directly in a minute quantity on the middle of the substrate, which is either at rest or rotating at a relatively low speed to enhance coating quality. Following that, the substrate is spun at a faster speed using the centrifugal force concept to enhance the coating speed. A spinner or spin coater is the machine used in this procedure [45].

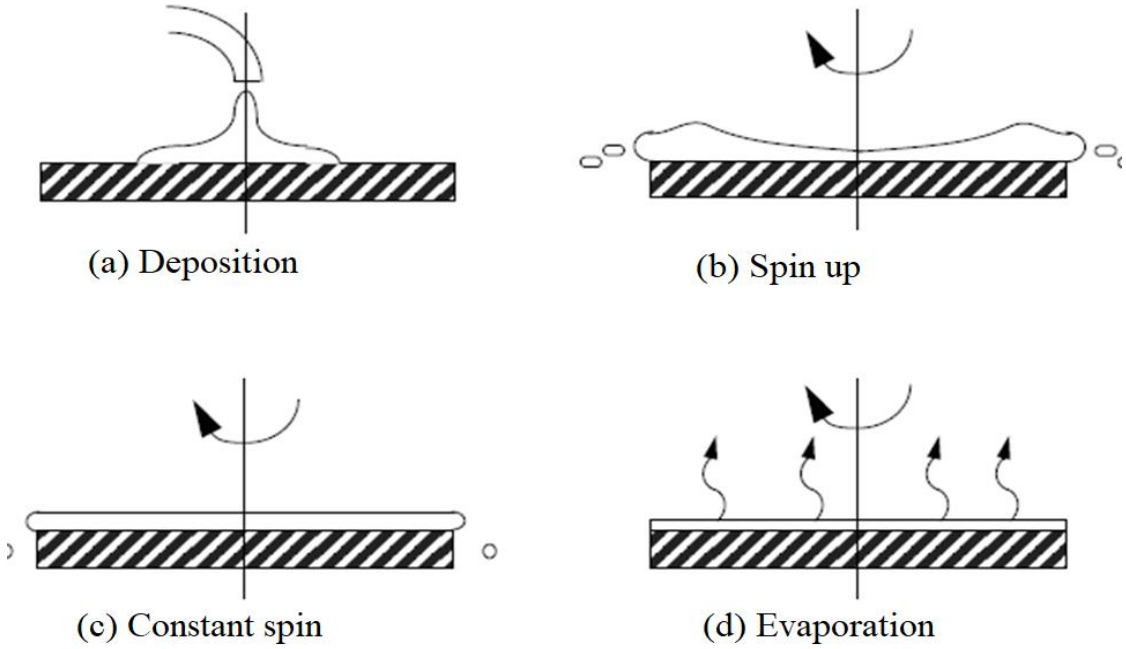

Figure 2.7: Schematics of spin coating

2.3.2 Sputtering

Sputtering is the process of ejecting atoms off a surface by showering them with high-velocity "positive" ions, mostly involving inert gas ions, and transferring momentum from the sputter gas to the atoms that need to be removed. The most frequent sputtering gas is argon. The released atoms condense and create a film on the substrate (which is a long way from the target). Sputtering yield is influenced by target composition, sputtering voltage, binding energy, and experiment geometry.

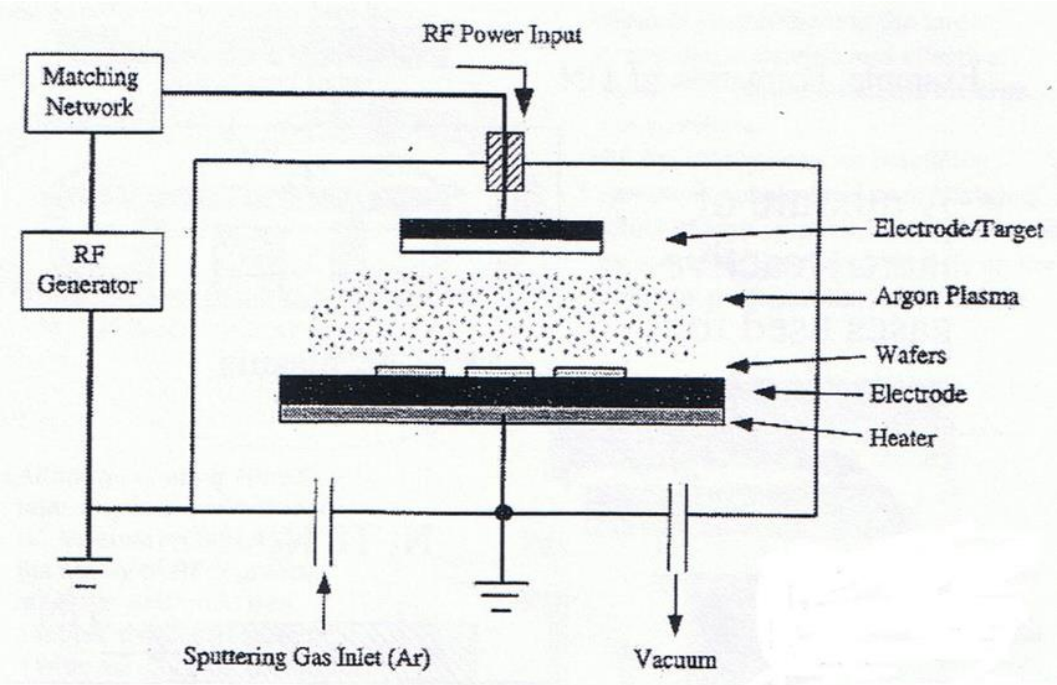

Figure 2.8: Schematics of sputtering

2.3.3 Chemical Vapor Deposition

This method of producing thin films was developed years ago. This process was originally adopted by dislodging in 1897 for deposition of tungsten on lamp filaments by reducing tungsten hexachloride with hydrogen. CVD is a robust extraction process because it generates highly pure materials. Gas molecules on the substrate are transformed into solid nanostructures (0D, 1D, 2D, 3D) in this chemical process. When the volatile precursors react/decompose on surface of substrate, desired coating is achieved.

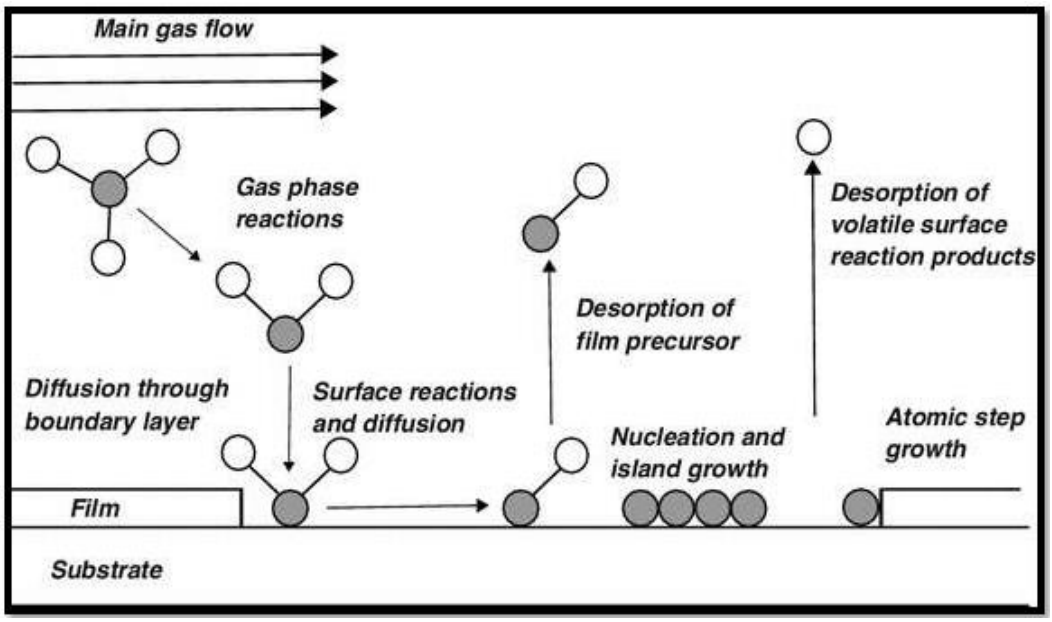

Figure 2.9: Schematics of CVD.

Chapter - 3

3 Methodology

3.1 Synthesis

Physical vapor deposition was used to deposit Au, TiO_2 and composite TiO_2/Au/TiO_2 thin films.

3.1.1 Preparation of Substrate

Silicon wafers are used to provide silicon wafers (100) that are roughly (2x2cm) in size. These silicon samples are used as substrates. The silicon wafer was cut into square substrates, which were then cleaned in ethanol for 30 minutes. In a beaker, substrates were dipped in ethanol and then suspended in an ultrasonic cleaner, which helps clean these substrates by stirring a liquid with high-frequency pressure (sound) waves.

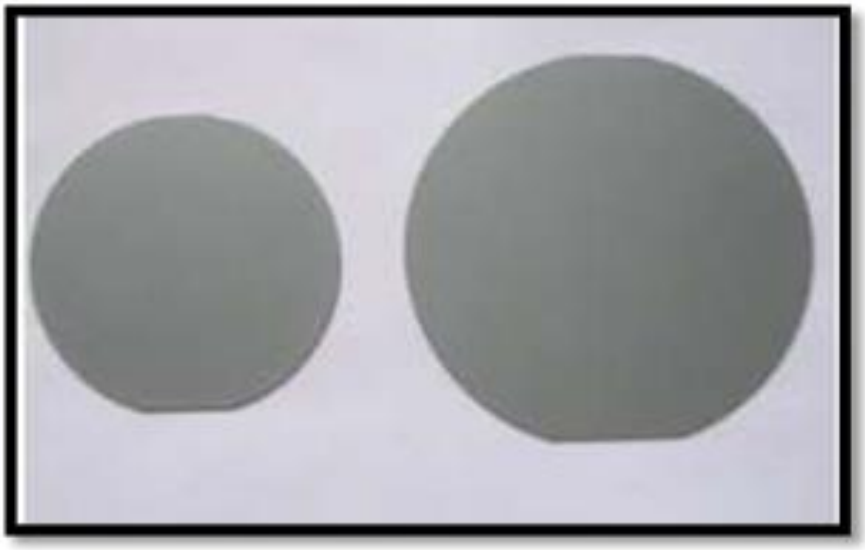

Figure 3.1: Silicon wafer

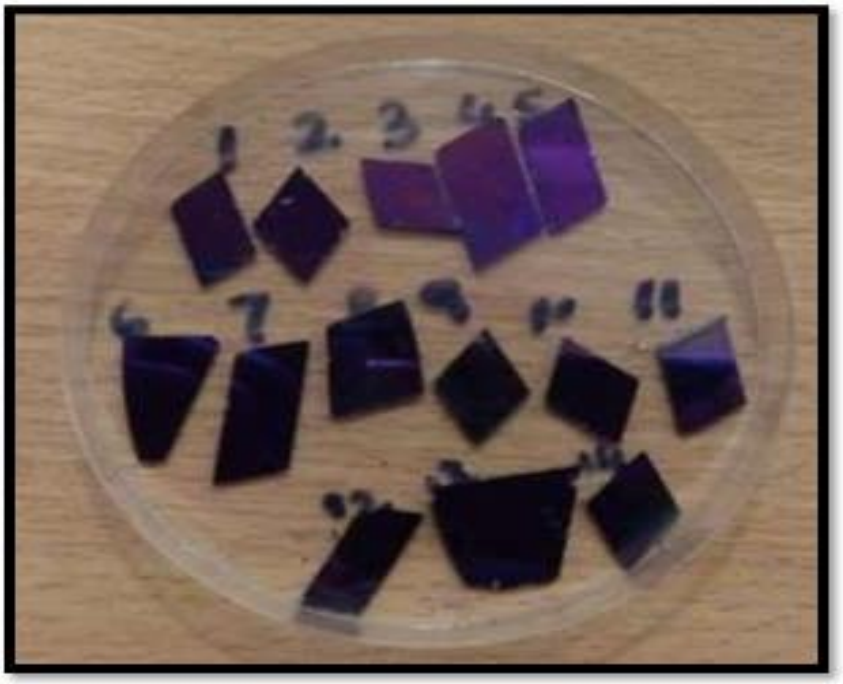

Figure 3.2: Silicon substrate

Figure 3.3: Ultrasonic cleaner

3.1.2 Deposition of TiO_2 Thin Films

In the first step powdered pallets of TiO_2 were placed as source material. Silicon substrate was placed in the substrate holder. The bell jar was connected to a high current source. A high vacuum of 10^{-5} torr was created inside the chamber. The current source was used to maintain an electrode current of 110 amp and 20nm TiO_2 was deposited at the rate of 0.2-0.3 nm/s. This method was repeated for 5 different samples and a base layer of 20nm TiO_2 was deposited for each sample.

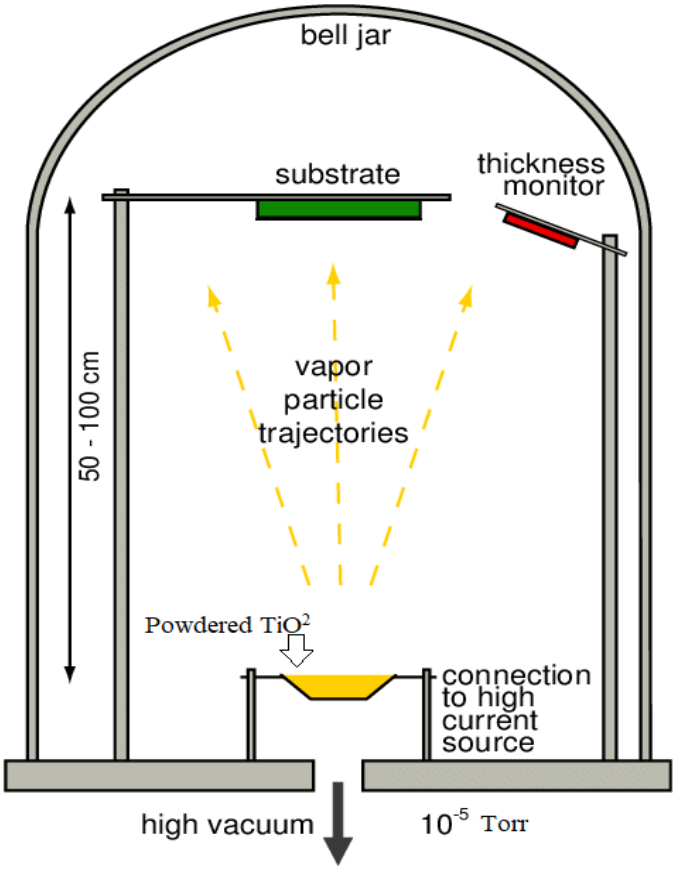

Figure 3.4: Deposition of TiO_2

3.1.3 Deposition of Gold Thin Films

In the second step, gold pallets were placed in the substrate holder. The substrate holder was connected to a high current source. A high vacuum of 10^{-5} torr was created inside the chamber. The current source was used to maintain an electrode current of 50 amp

and gold was deposited at the rate of 0.1 nm/s. This method was repeated for all 5 different samples in order to deposit gold layers with different thicknesses i.e. 1nm, 3nm, 5nm, 10nm, 20nm on 20nm base layer of TiO_2.

3.1.4 Deposition of TiO_2 Thin Films

The third and final step of this process was done by again placing TiO_2 pallets as source material. Silicon substrate was placed in the substrate holder. The substrate holder was connected to a high current source. A high vacuum of 10^{-5} torr was created inside the chamber. The current source was used to maintain an electrode current of 110 amp and 20nm TiO_2 was deposited at the rate of 0.2-0.3 nm/s. This method was repeated for all 5 different samples and a final layer of 20nm TiO_2 was deposited for each sample. For ease of use, we named these samples as Au1, Au3, Au5, Au10 and Au20 referring to 1nm, 3nm, 5nm, 10nm and 20nm thicknesses of Au. Deposition steps were performed to form composite structures as shown in the figures.

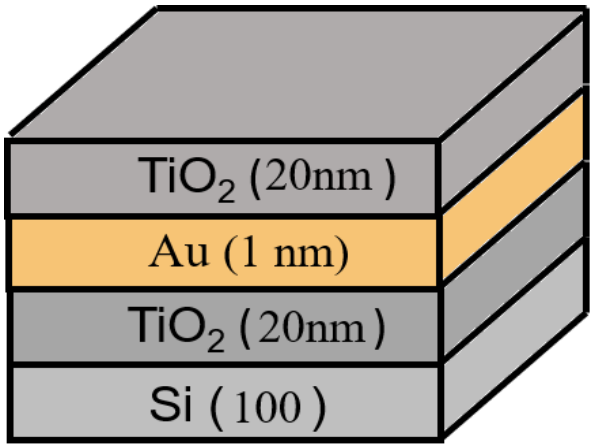

Figure 3.5: Composite films with 1nm Au thickness (Au1)

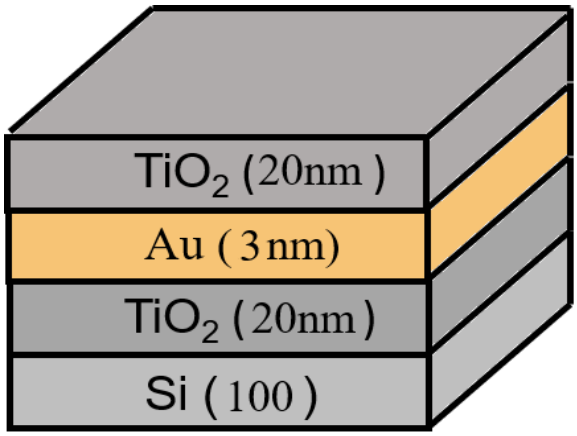

Figure 3.6: Composite films with 3nm Au thickness (Au3)

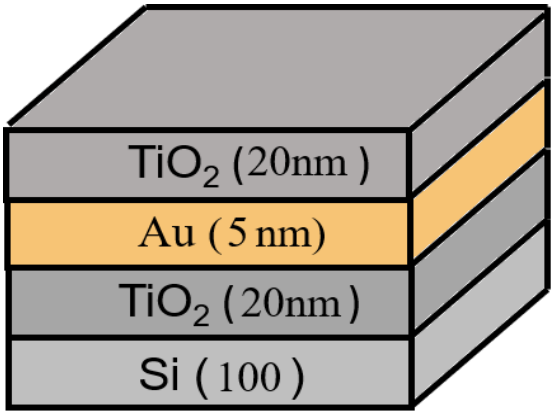

Figure 3.7: Composite films with 5nm Au thickness (Au5)

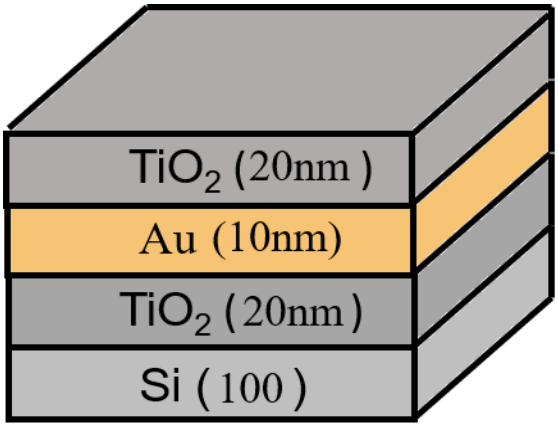

Figure 3.8: Composite films with 10nm Au thickness (Au10)

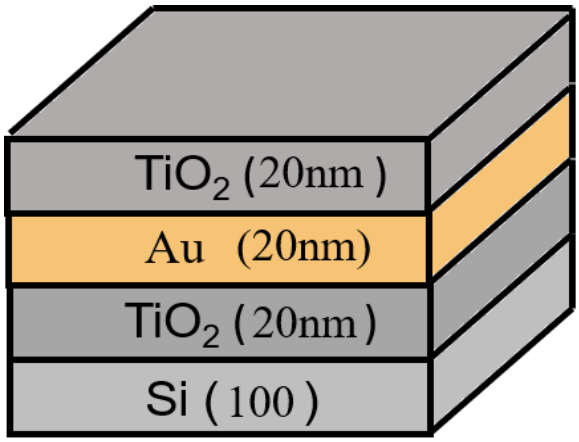

Figure 3.9: Composite films with 20nm Au thickness (Au20)

3.2 Characterization Techniques

Following characterization techniques were employed on the composite structures to learn about their thickness, composition and optical properties.

3.2.1 Spectroscopic Ellipsometry

It is a non-destructive and non-invasive technique for analyzing a sample's optical characteristics. It obtains data by determining the relative change in polarization of the incident and reflected signal and hence is uninfluenced by the absolute intensity of the incident light. The thickness of a sample may be measured with spectroscopic ellipsometry within the resolution of a few nanometres. It also includes information on transmission, absorption, reflection, complicated refractive and dielectric functions, and many other optical characteristics.

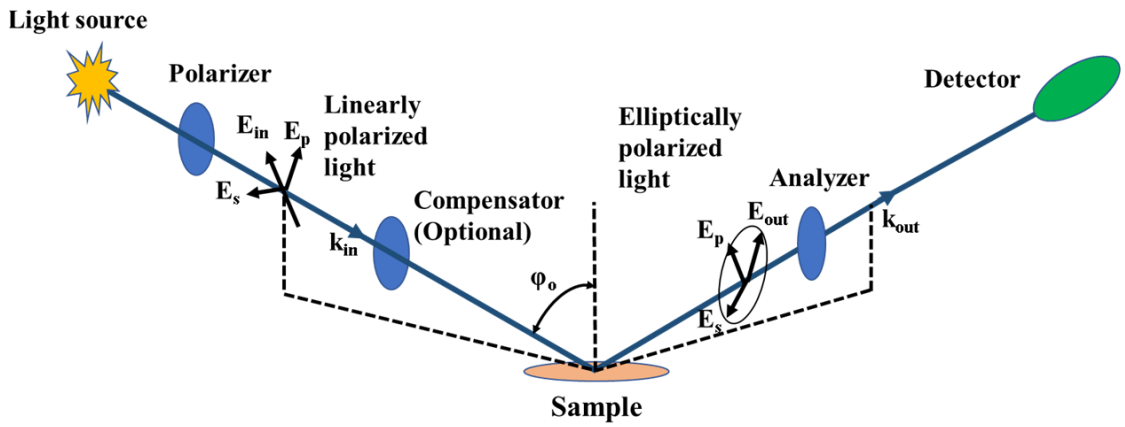

Figure 3.10**:** Schematic of a spectroscopic ellipsometery

Figure 3.10 shows the basic schematic of how ellipsometry works. It shows the fall of an incoming beam of light on a sample with two orthogonal electric field components parallel and perpendicular with respect to the plane of incidence. The plane of incidence is parallel to the incident light propagation direction and perpendicular to the sample's surface. A vector 'k_{in}' represents the propagation direction of incoming light. The amplitude and state of polarization, changes after reflection from the sample's surface. As a result, the reflected signal 'k_{out}' is elliptically polarized. Xe lamp with high-pressure is used for incident light. Filters are employed to obtain a spectrum of 200-800 nm by acquiring the signal at the required wavelength. The amplitude ratio and phase change of the incoming light are acquired as raw data from ellipsometry. The incident light's shift in s and p-polarization states is measured. Polarizer (P)- compensator (C)- sample (S)- analyzer (A), sometimes known as PCSA, are the fundamental components necessary to perform ellipsometry measurements. The light of any state is converted into a linearly polarized state by a linear polarizer positioned in front of the sample. The limitations of ellipsometry include light being obliquely incident on the material, and the spot size being several millimeters in diameter, reducing spatial resolution. Furthermore, the sample's reflection must be greater than the dispersed signal for the signal to be optically recorded. The amplitude ratio and phase change curves are then fitted to theoretical models, and different optical characteristics such as absorption, reflection, complicated refractive, and dielectric functions are retrieved.

3.2.2 Raman Spectroscopy

It is a characterization method that involves the inelastic scattering of photons when a laser source is incident on a material. Inelastic scattering is a phenomenon in which the frequency radiated by atoms or molecules is red or blue shifted compared to the frequency absorbed. The photons from the laser source are absorbed by the object, which then begins to emit again. The Raman Effect occurs when there is a difference in the frequency of absorbed and reemitting photons. The vibrational, rotational, and other low frequency scatterings in crystal structure are described by this shift in frequency. The crystallinity and structure of the produced material can be determined using Raman spectroscopy. This characterization technique is used to detect defects, impurities, structural damage, and residual stresses. The structure and motions of the studied system are revealed by photon interaction with material. When an incident photon hits the material, it excites its atoms or molecules from their ground state to an excited state. It then experiences two types of Raman scatterings when it de-excites.

3.2.2.1 Stokes Scattering

Stokes scattering occurs when an atom or molecule returns to a final vibrational state with energy higher than the initial state. Anti-Stokes scattering happens when an atom or molecule returns to a final vibrational state with energy less than the initial state.

3.2.2.2 Anti-Stokes Scattering

Anti-Stokes scattering occurs when an atom or molecule returns to a final vibrational state with less energy than the initial state.

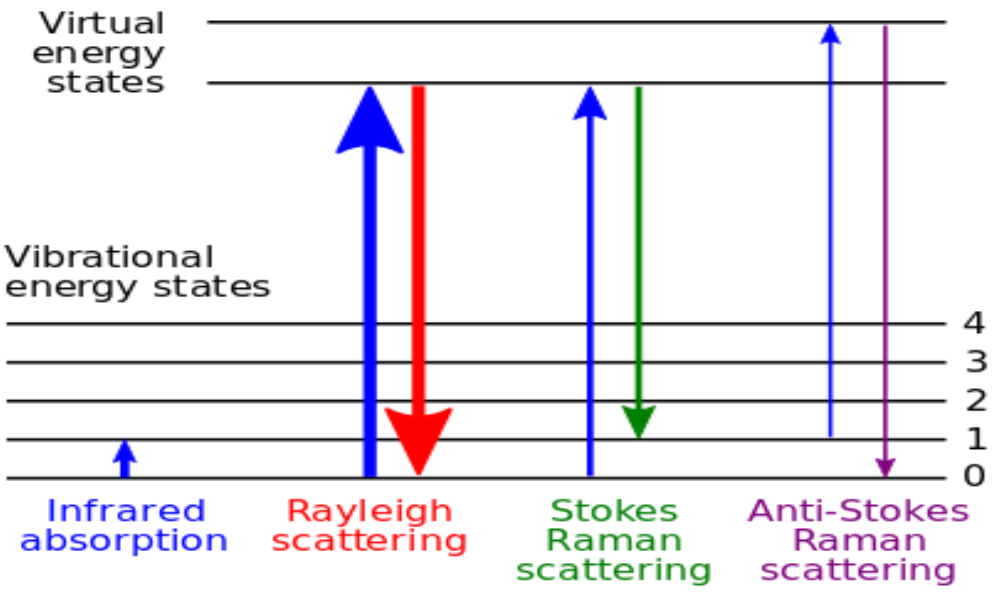

Figure 3.11: Stokes and Anti-Stokes Raman scatterings

3.2.3 Photoluminescence Spectroscopy

Photoluminescence spectroscopy is used to measure the spontaneous emission of light from the material after the light is incident on it. It is a contactless, non-destructive technique and does not require any sample treatment or preparation. Figure 3.12 shows a schematic for the photoluminescence process in a direct band gap semiconductor.

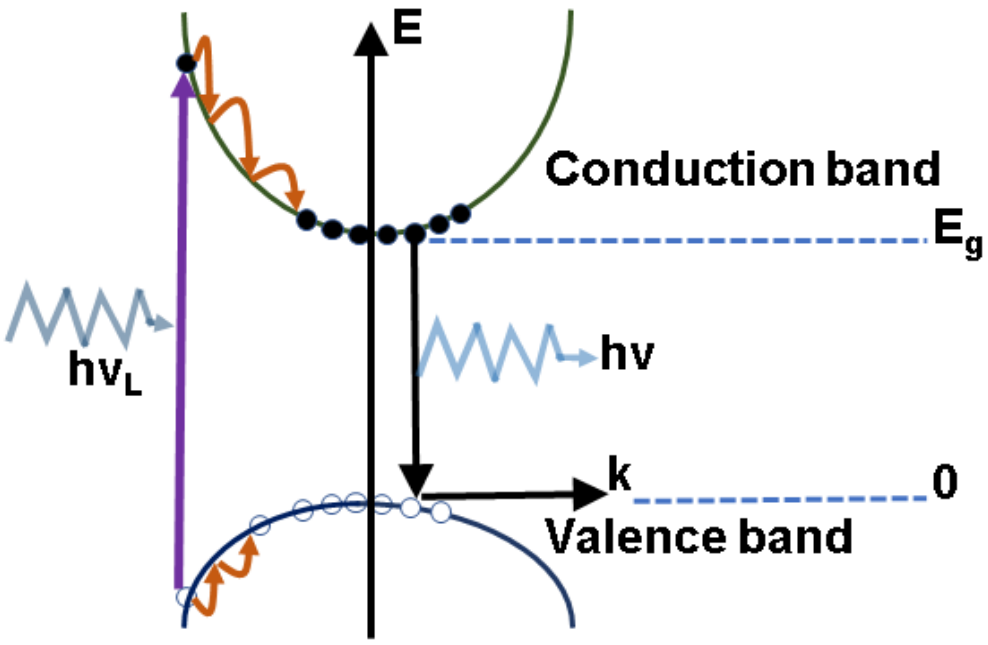

Figure 3.12**:** Schematic for radiative transitions in a direct band gap semiconductor.

When a sample is hit by laser light with an energy larger than the band gap, an excited electron is generated in the conduction bad and an excited hole is generated in the valence band. These excited charge carriers approach the conduction and valence band minima and maxima, respectively, and recombine radiatively later. These transitions give information regarding the structure's electronic energy levels. PL spectroscopy can also be used to determine information about the structure's interfacial/surface defect states.

3.2.4 Ultraviolet-visible Spectroscopy

UV/Vis spectroscopy is used to analyze the absorption or reflectance behavior in the UV and visible spectral range. Absorption or reflectance in the visible range of electromagnetic spectrum in a straight line affects the apparent color of the materials involved. Atoms and molecules undergo electronic transitions over the electromagnetic spectrum.

Fluorescence and absorption spectroscopy are coupled in fluorescence spectroscopy, with fluorescence accounting for conversions from the ignited state to the ground state

and absorption accounting for evolutions from the ground state to the excited state. The visible region is made up of photons with energy ranging from 36 to 72 kcal/mole.

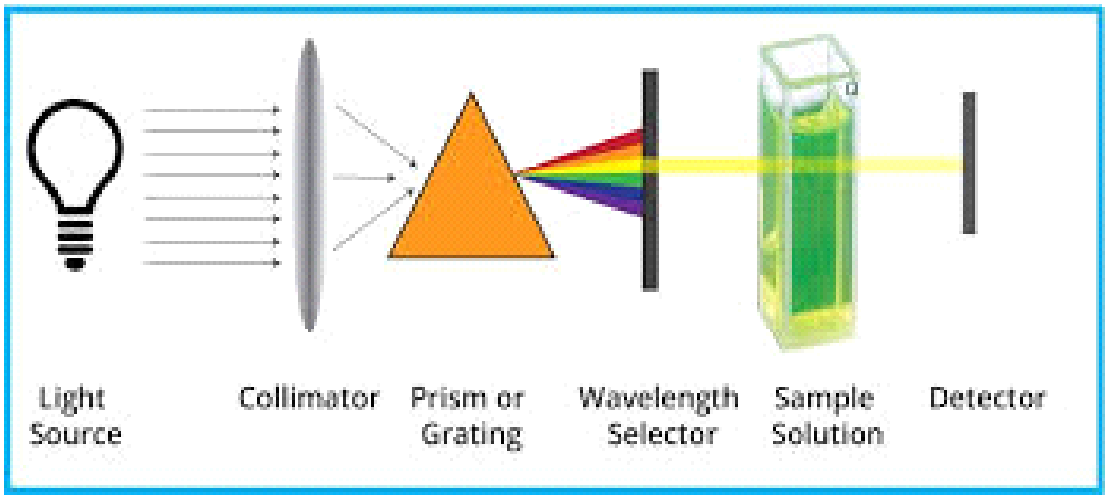

Figure 3.13: Schematic of UV/Vis

3.2.5 Atomic Force Microscopy (AFM)

Surface morphology and thin film roughness are detected using AFM, which is a powerful technique. AFM investigates the number of graphene layers, homogeneity, and topography. The sharp tip of the AFM probe is positioned on a cantilever spring. Atomic forces between the sample and the tip deflect the cantilever. The laser beam records the reaction of atomic forces as the cantilever moves across the surface, focusing on the tip. After traveling through a succession of mirrors and lenses, the beam bounces off the cantilever and is focused on the photodiode detector. The photodiode's signal is delivered to the piezoelectric tube, which houses the cantilever. Changing the height of the piezo tube maintains the cantilever's deflection. The surface response of the piezoelectric crystal is stored and collected as an image as the tips raster scans [46].

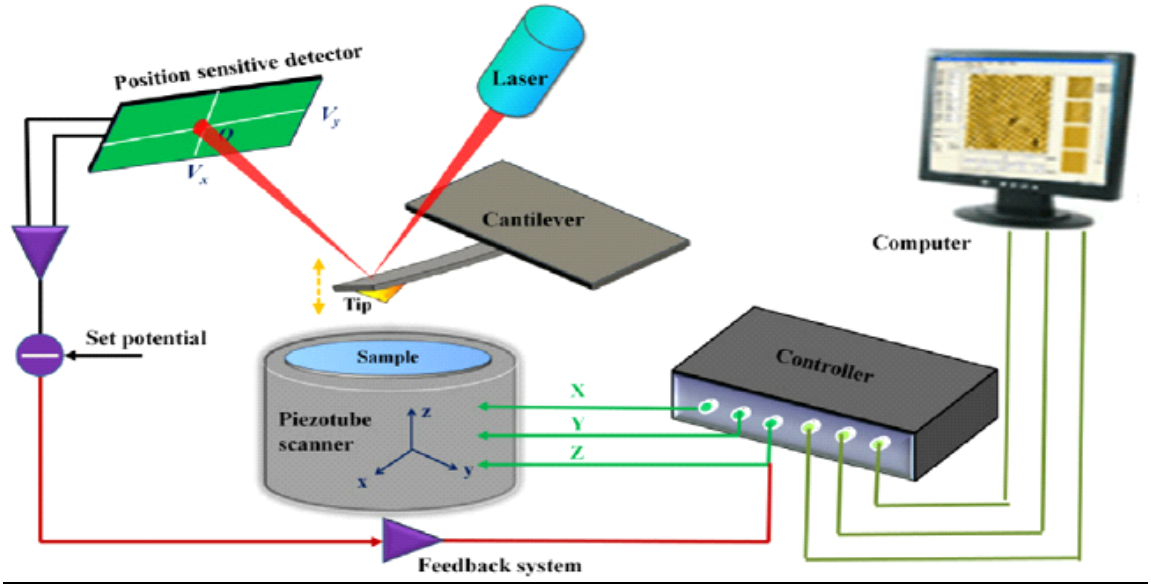

Figure 3.14: AFM Schematic diagram

AFM consists of three different modes which are contact mode, non-contact mode and tapping mode.

3.2.5.1 Contact mode

In contact mode, the microscope's tip sweeps the sample with the sample and tip in close proximity of contact, resulting in an average force of 10 -9 N. The cantilever's force on the sample surface is constant, but its position is altered by the piezoelectric arrangement factor. The cantilever's rebound is initially investigated, followed by a comparison with feedback from a direct current amplifier to a specified level of deflection. This is how AFM contact mode functions. If the computed deflection does not match the supplied value, voltage is applied to the Piezo via a feedback amplifier to raise or lower the deflection. The voltage applied by the feedback amplifier at the Piezo is essentially a measurement of the sample's surface properties. In samples including semiconducting and insulating materials, a large quantity of electrostatic charge can be trapped. This stored charge contributes to additional forces of attraction between the probe and the sample. These forces have the potential to harm samples, dull the cantilever probe, and distort the ensuing data. Non-contact mode can be used to prevent this issue.

3.2.5.2 Non-contact mode

The non-contact mode boundaries tip hovers 50-150 angstrom beyond the sample's surface. Attractive Van der Waals forces exist between the tip and the provided sample, and they are identified here. Topographic images are created when the tip is scanned above the surface. Unfortunately, attractive forces are substantially more brittle than forces applied in contact mode. As a result, in order to employ the AC detection method to represent small forces between tip and sample via measurement of sample change, the tip must exhibit minimal oscillation. The use of Van der Waals forces to measure force gradients is unavoidable. These forces may only be a nanometer away from a sample's surface. It is impossible to create accurate images for a layer with a thickness greater than the Van der Waals force range.

3.2.5.3 Tapping Mode

This mode is used for high-resolution imaging of surfaces that are prone to damage, have a poor bond to the substrate's surface, or are difficult to scan with the other two AFM modes. This AFM mode overcomes issues such as friction, adhesion and electrostatic forces, etc. In this mode, the tip touches the material surface to acquire high resolution before being animated away from the surface to prevent dragging. A piezoelectric crystal is used to oscillate the cantilever assembly at the cantilever's resonance frequency, enabling outside imaging. The cantilever oscillates with a sizable amplitude (usually greater than 20nm) when the piezo motion is present as long as the tip is not in contact with the surface. After that, the oscillating point is moved closer to the surface until it lightly contacts or taps it. During tapping mode operation, a feedback loop keeps the cantilever-oscillation amplitude constant. With the aid of software, the appropriate oscillation frequency is chosen, and the force acting on the sample is adjusted and kept at the minimum amount. When the tip touches the surface, its oscillation amplitude is sufficient to overcome the adhesion forces between the tip and the sample. It also has a large linear operating range, which is a plus.

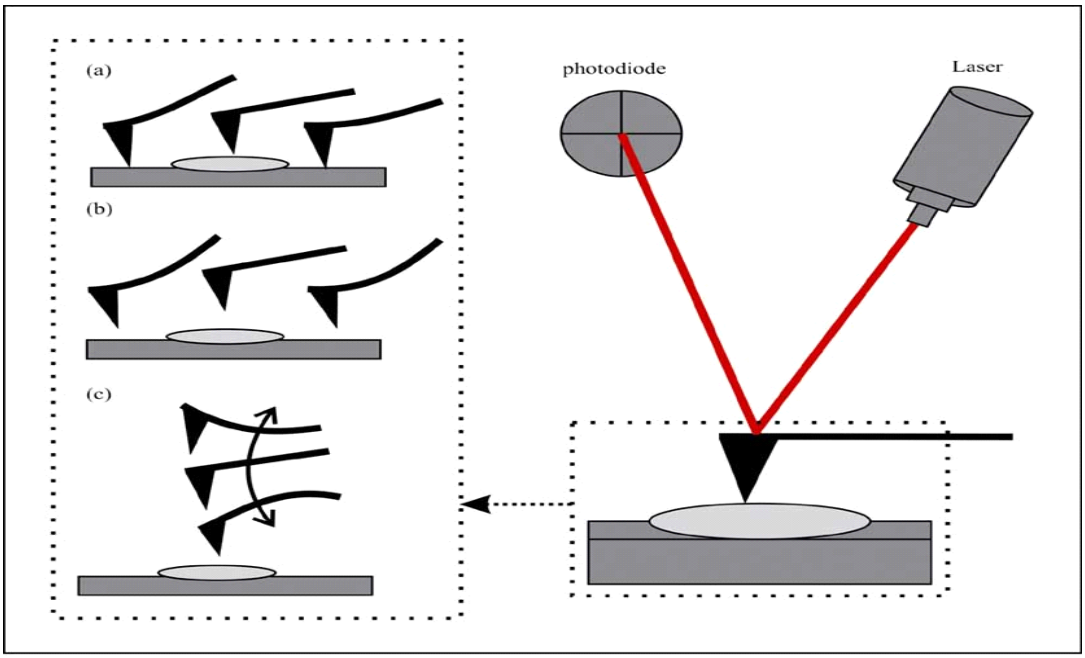

Figure 3.15: (a) Contact Mode (b) Non-Contact Mode (c) Tapping Mode [47].

Chapter - 4

4 Results and Discussion

In this chapter, a detailed analysis by different characterizations of experimental results is obtained and explained. The structural morphology and properties of TiO_2/Au/TiO_2 nanocomposite films are also discussed in this chapter.

4.1 Raman Spectroscopy

Raman spectroscopy shows that the first peak exists at 139.6 cm^{-1}, the second peak is found at 396.7 cm^{-1}, the third peak is located at 516.9 cm^{-1} and the fourth peak was found to be at 641.5 cm^{-1}. These modes correspond to E1g, B1g, A1g, and Eg3. When it comes to molecular vibrations, Group Theory utilizes a notation in which one-dimensional representations are represented by A or B, two-dimensional representations are denoted by E, and three-dimensional representations are denoted by T. The Eg bands, B1g band, and A1g mode in TiO_2 are all brought about by symmetric stretching vibrations of O-Ti-O, symmetric bending vibrations of O-Ti-O, and antisymmetric bending vibrations of Ti-O-Ti. However, the creation of the long-range order anatase phase is confirmed by the strongest well-resolved mode at 139.6 cm^{-1} increased due to external symmetric vibration [48].

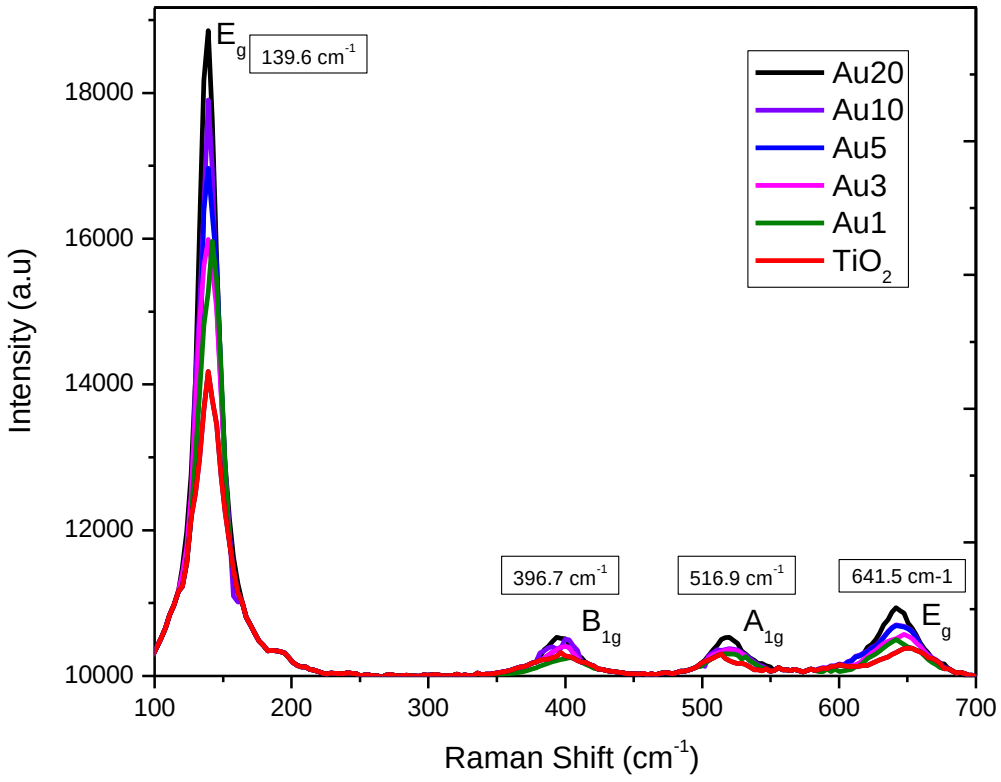

Figure 4.1: Raman Spectra of TiO_2 and composite films

4.2 Atomic Force Microscopy (AFM)

AFM was used to examine the surface structure of deposited composite films on a silicon substrate. Morphology of deposited film plays a critical role in modulating the band gap of materials thereby inflicting a change in energy harvesting properties. Figures show the smoothness of the layers deposited which played an important part in altering the optical properties of TiO_2. Average roughness for Au1, Au3, Au5, Au10 and Au20 was found to be 22.19 nm, 18.20 nm, 28.42 nm, 38.87 nm and 25.97 nm respectively.

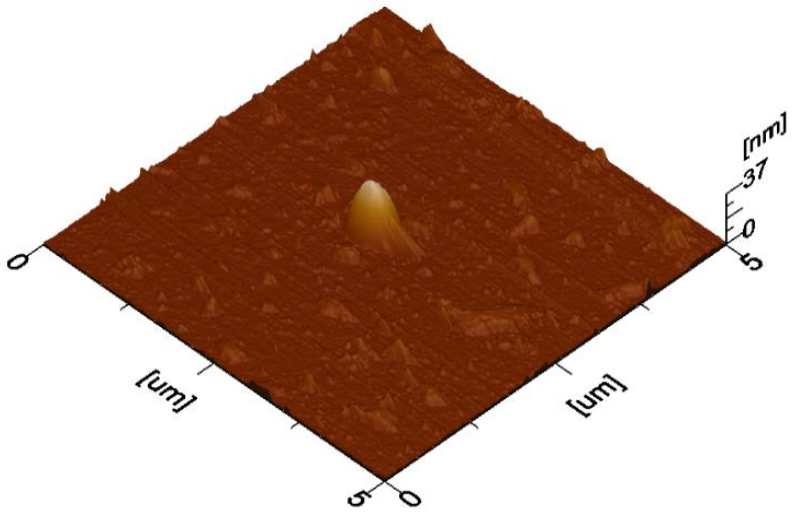

Figure 4.2: AFM image of Au1

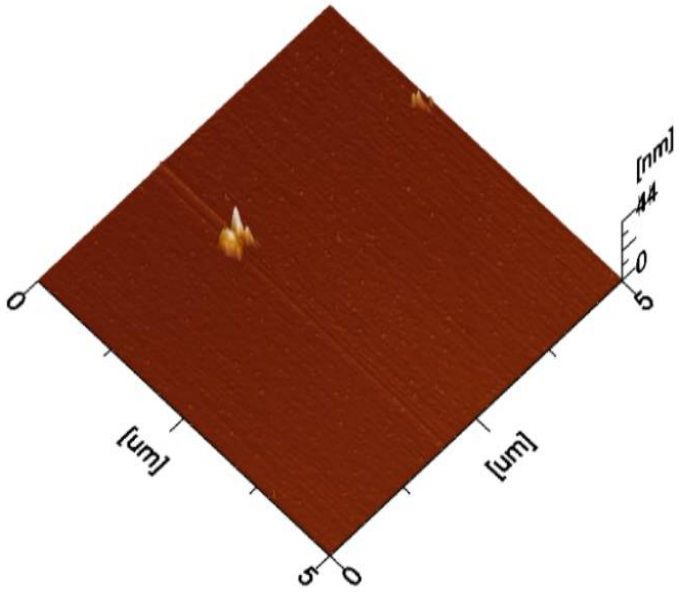

Figure 4.3: AFM image of Au3

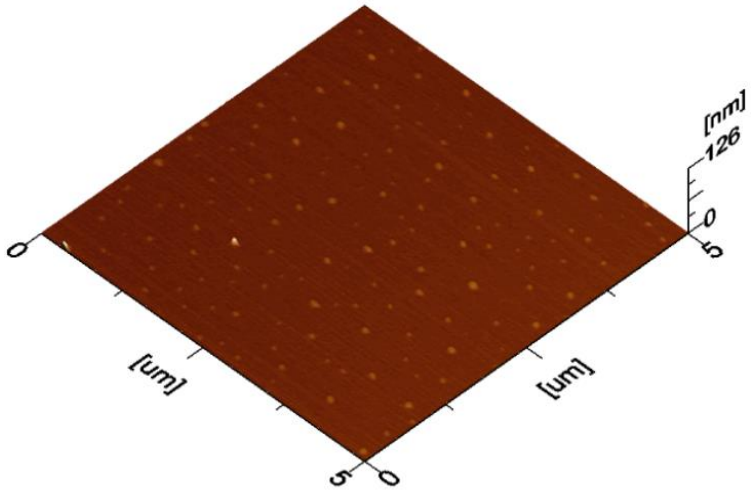

Figure 4.4: AFM image of Au5

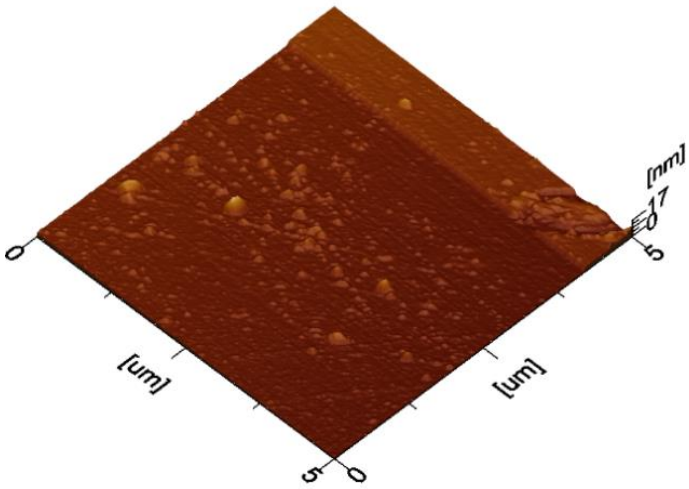

Figure 4.5: AFM image of Au10

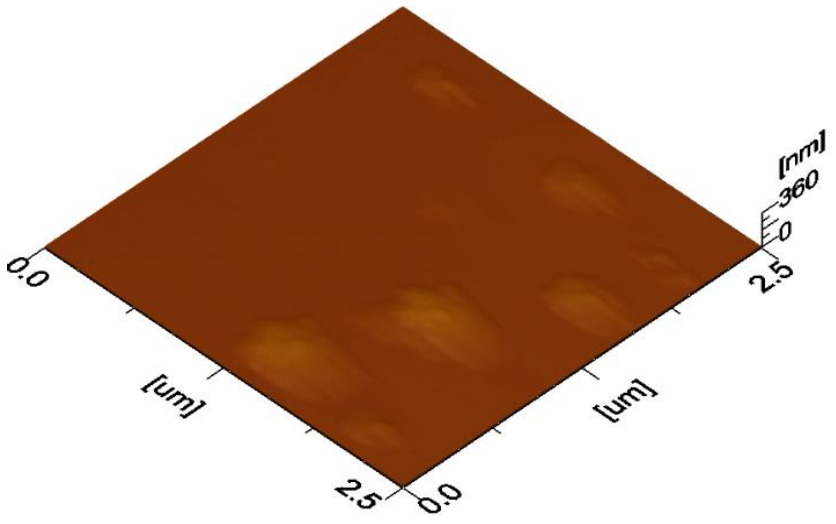

Figure 4.6: AFM image of Au20

4.3 Photoluminescence Spectroscopy

Photoluminescence spectroscopy was employed to analyze the optical properties of the Au sandwiched thin film. A 325 nm He-Cd laser was used for photoluminescence spectroscopy, and the scattered intensity was measured with a LabRam III, DongWoo, Optron PL spectrometer. Photoluminescence spectroscopy of TiO_2/Au/TiO_2 thin films are shown in figure 4.6.

The band edge emission peak which can be observed in TiO_2 had an additional peak in TiO_2/Au/TiO_2 films. This observation showed the presence of near band edge defects and the introduction of tail states in TiO_2. In TiO_2 thin films and nanostructures, there are 3 different types of luminescent centers: direct band to band permitted transitions in

the UV region (~351 nm), oxygen defects at roughly 520 nm, and Tin+ multivalent ionic states in the infrared range.

In TiO_2 samples, all 3 types of luminescent centers were present. Due to electrons injected through the surface plasmon resonance phenomenon, photoluminescence spectroscopy indicated the maximal pinning of defect states in the TiO_2 interface. [49].

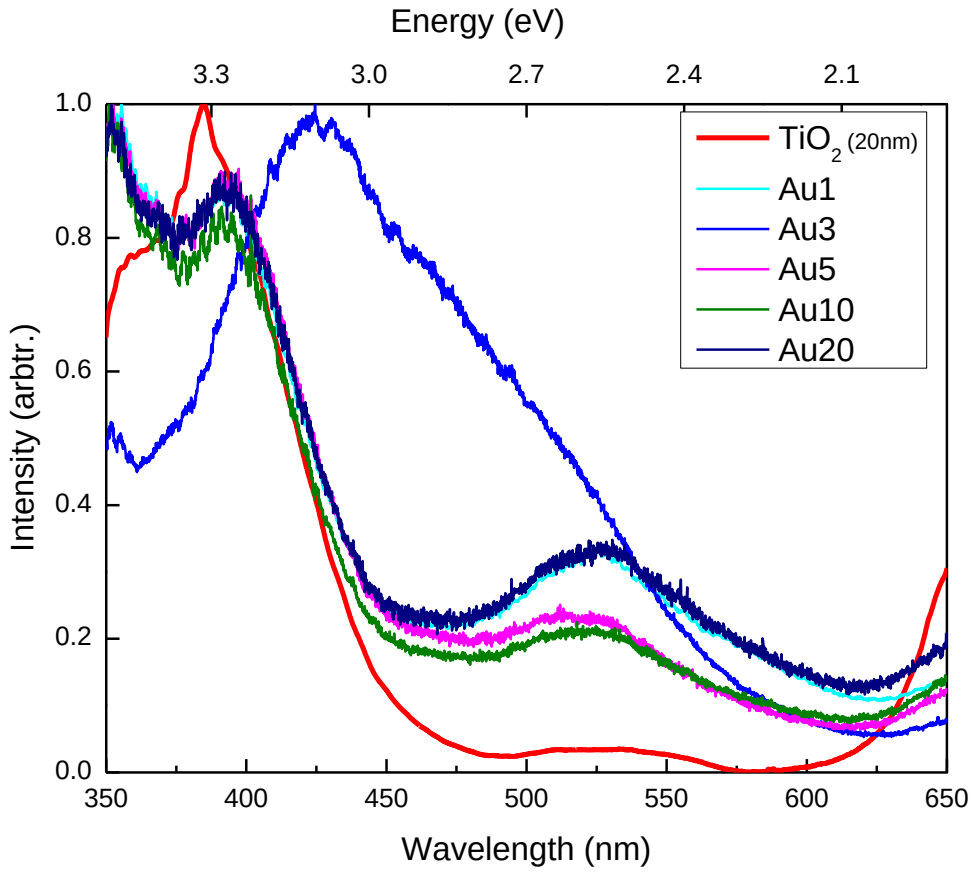

Figure 4.7: Photoluminescence spectra of TiO_2 and TiO_2/Au/TiO_2 composite films

4.4 Spectroscopic Ellipsometry

The optical characterization of Au sandwiched thin film was done using spectroscopic ellipsometry. Spectroscopic ellipsometry was performed using SENTECH Instrument, GmbH (SE 850). The model was fitted using SpectraRay to analyze thicknesses of TiO_2 layers and Au layer and TiO_2/Au/TiO_2 layers deposited. Experimental data were fitted to

theoretical data to obtain the maximum approximation of thickness of composite films. The amplitude ratio and phase change of the incoming light were acquired as raw data from ellipsometry. The model used to estimate the thicknesses of each layer in composite films is shown in figure 4.7.

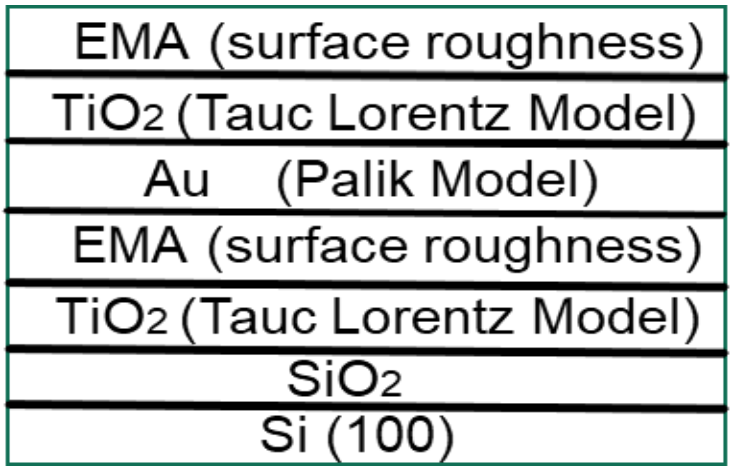

Figure 4.8**:** Modeled layered structures of thin films for Spectroscopic Ellipsometry of composite films

Experimental data was fitted to theoretical data to obtain maximum approximation of thickness of TiO_2/Au/TiO_2 thin films. The thicknesses of layers in Au1 were found to be 20/1/20 nm for TiO_2/Au/TiO_2 only. For Au1 raw experimental and theoretical data fitted is show in figure 4.8.

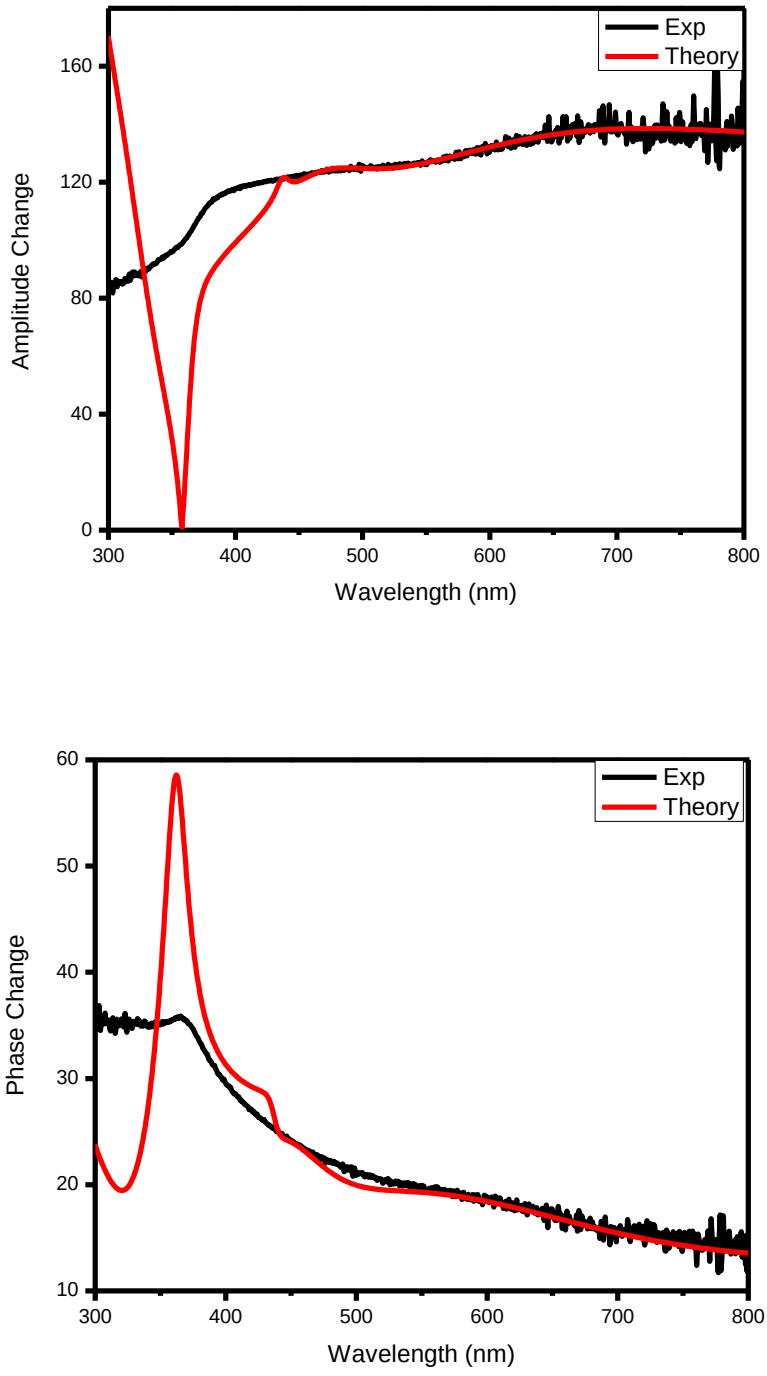

Figure 4.9: Amplitude ratio plots of Au1. Phase change plots of Au1

The thicknesses of layers in Au3 were found to be 20/3/20 nm for TiO_2/Au/TiO_2. For Au3 raw experimental and theoretical data fitted is show in figure 4.9.

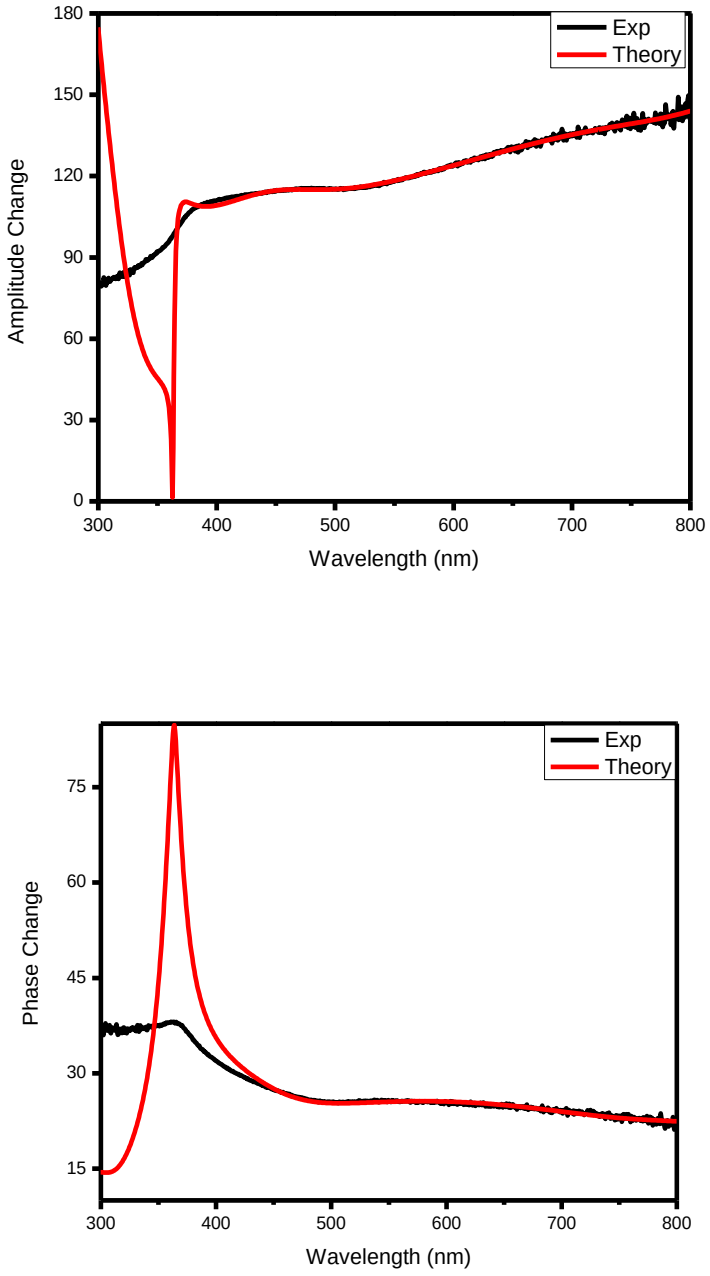

Figure 4.10: Amplitude ratio plot of Au3. Phase change plot of Au3.

The thicknesses of layers in Au5 were found to be 20/5/20 nm for TiO_2/Au/TiO_2. For Au5 raw experimental and theoretical data fitted is show in figure 4.10.

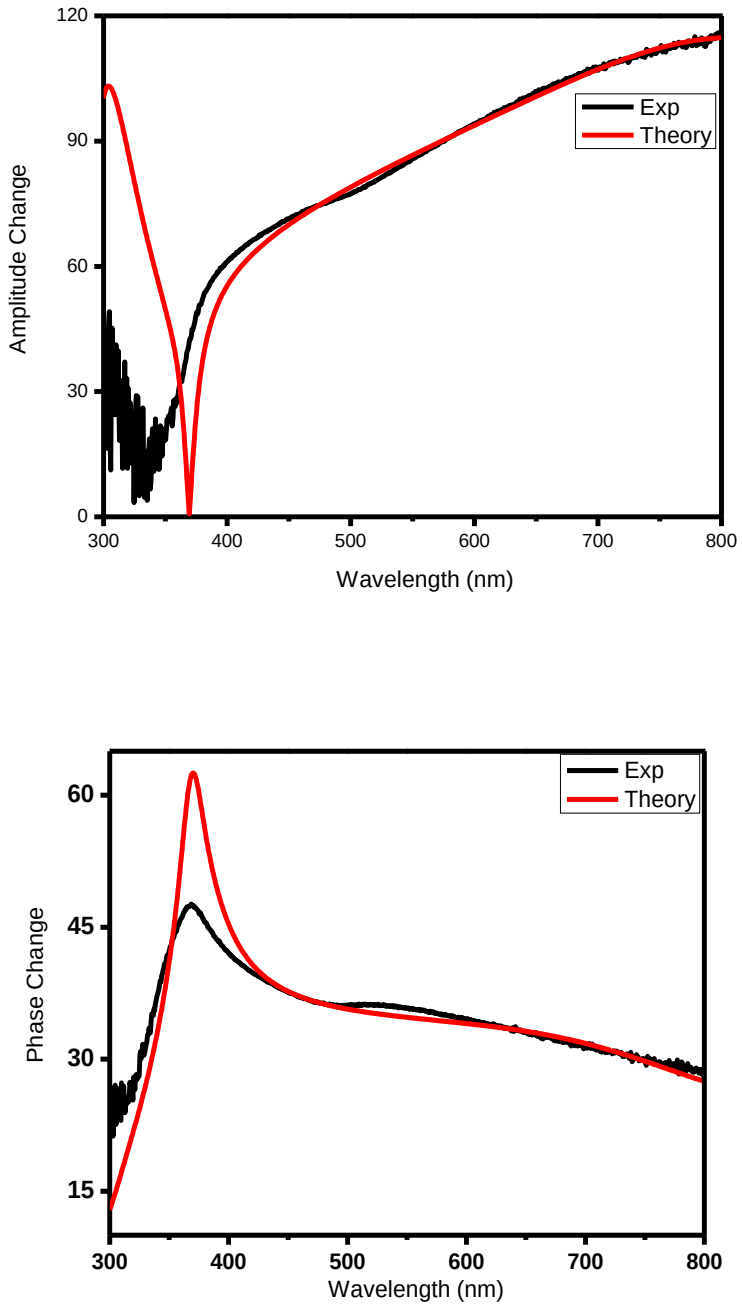

Figure 4.11: Amplitude ratio plot of Au5. Phase change plot of Au5.

The thicknesses of layers in Au10 were found to be 20/10/20 nm for TiO_2/Au/TiO_2 only. For Au10 raw experimental and theoretical data fitted is show in figure 4.11.

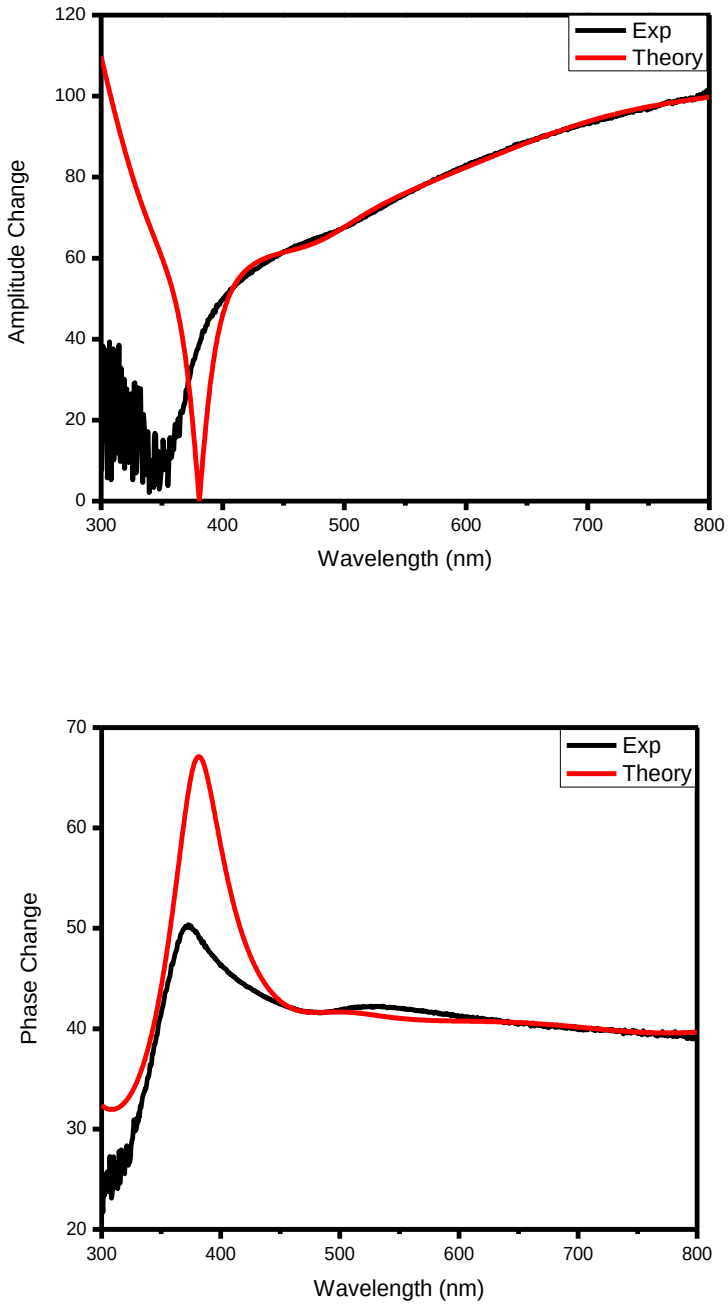

Figure 4.12: Amplitude ratio plot of Au10. Phase change plot of Au10.

The thicknesses of layers in Au20 were found to be 20/20/20 nm for TiO_2/Au/TiO_2 only. For Au20 raw experimental and theoretical data fitted is show in figure 4.12.

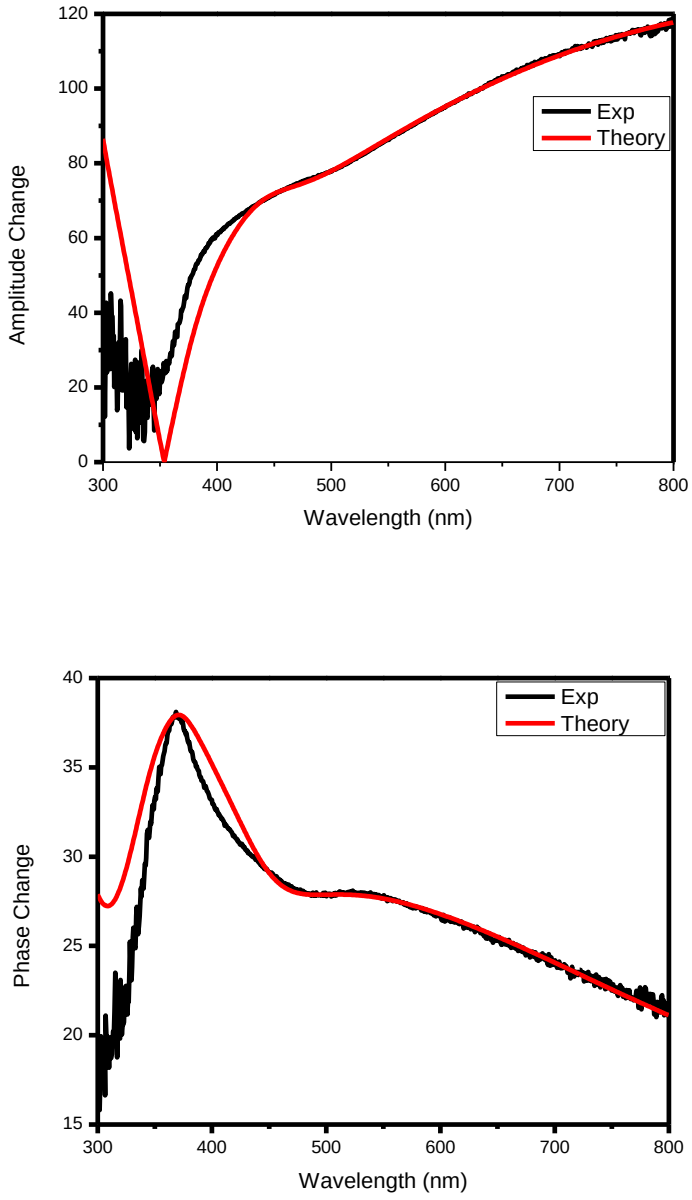

Figure 4.13: Amplitude ratio plot of Au20. Phase change plot of Au20

4.5 Ultraviolet-Visible Spectroscopy (UV/Vis)

UV/Vis absorption spectroscopy in part of the ultraviolet and the visible spectral regions was done. The $TiO_2/Au/TiO_2$ composite film showed an increased absorption in the visible region specifically for composite films with 1nm Au and 3nm Au thicknesses around 420nm marked as A. As the thickness of Au layer is increasing, this enhanced absorption can be seen decreasing. These peaks around 420nm are due to interband transitions. Au with 5nm resulted in a weak band around 730nm due to surface plasmon resonance mode marked as B. Au with thickness 10nm and 20nm depicted a band around 670nm and 620nm respectively due to SPR mode marked as C. As the thickness of the Au layer is increasing, the SPR is shifting towards smaller wavelength.

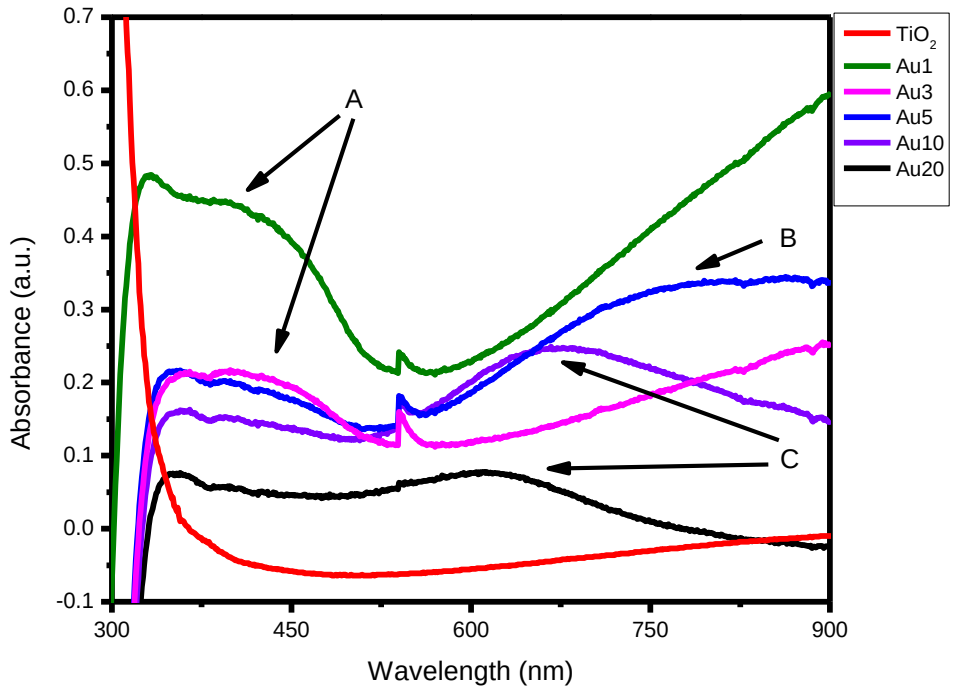

Figure 4.14: UV/Vis absorption spectroscopy of TiO_2 and composite $TiO_2/Au/TiO_2$ thin films.

The energy band gap of TiO_2/Au/TiO_2 films was clearly modified as obtained by Tauc plots. For Au1 this was decreased up to 1.7 ± 0.1 eV which was a drastic change in band gap compared to other samples. For Au3, band gap was reduced to 2.0 ± 0.1 eV. For Au5, band gap was tuned to 2.2 ± 0.1 eV. For Au10, band gap was found to be 2.3 ± 0.1 eV. For Au20, band gap was found to be 2.3 ± 0.1 eV. An increase in band gap can clearly be seen with an increase in thickness of Au layer hence conclusion is that the 1nm layer of Au plays the best role in modifying optical properties of TiO_2 and with the increase in thickness of Au layer, TiO_2 shows lesser absorption in the UV/Vis range.

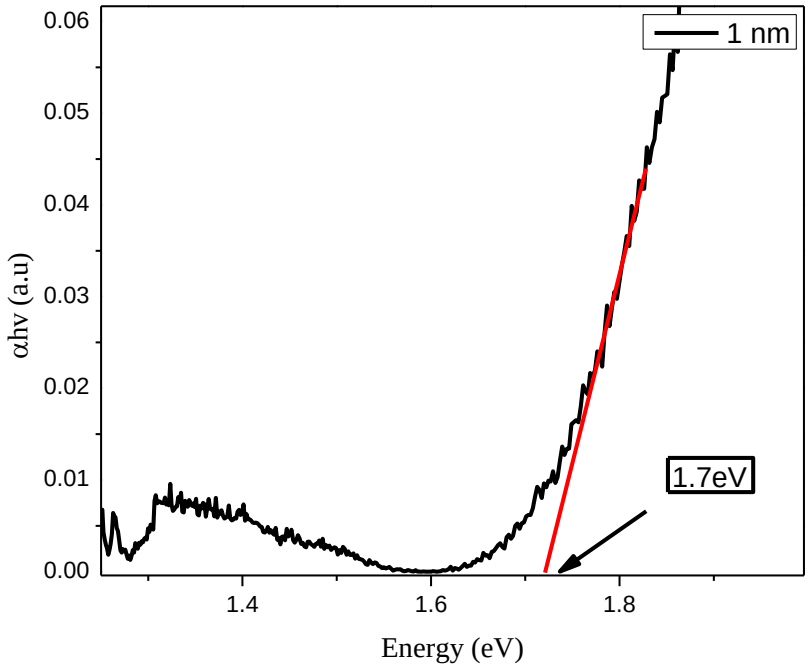

Figure 4.15: Tauc plot of Au1

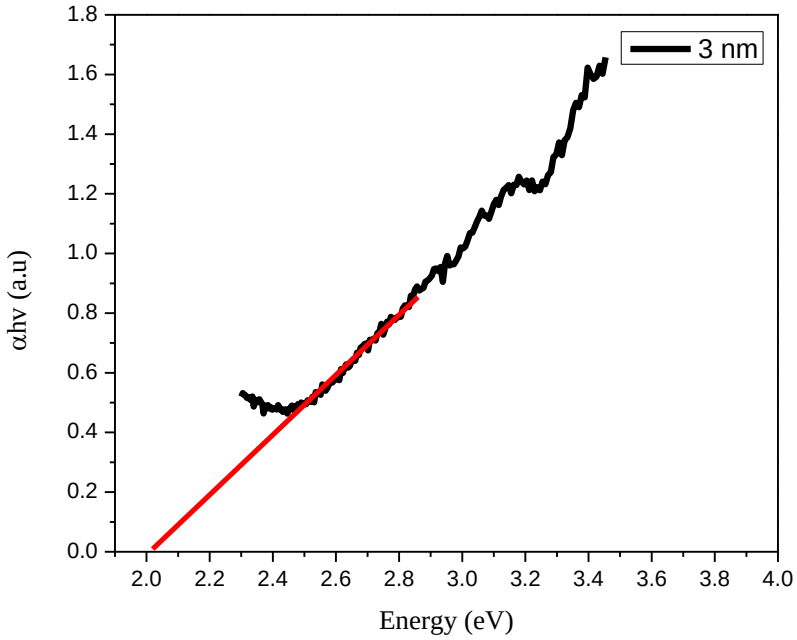

Figure 4.16: Tauc plot of Au3

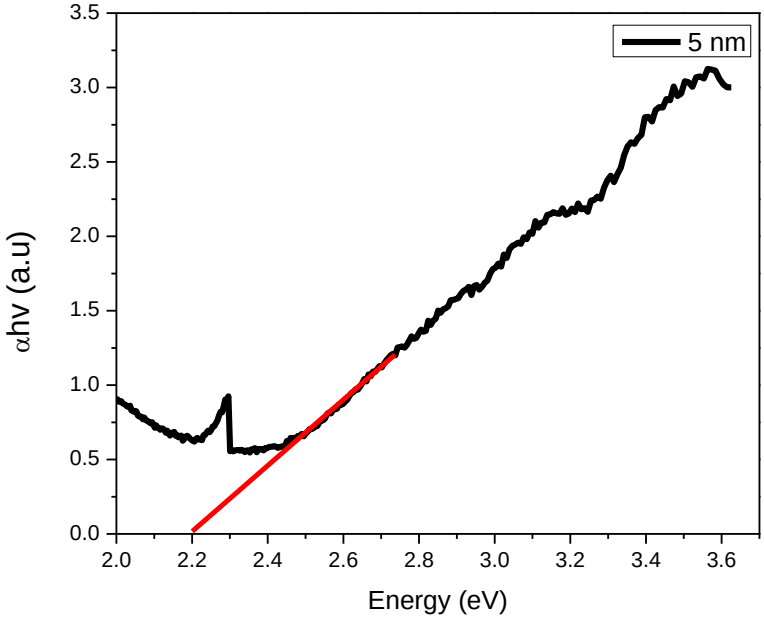

Figure 4.17: Tauc plot of Au5

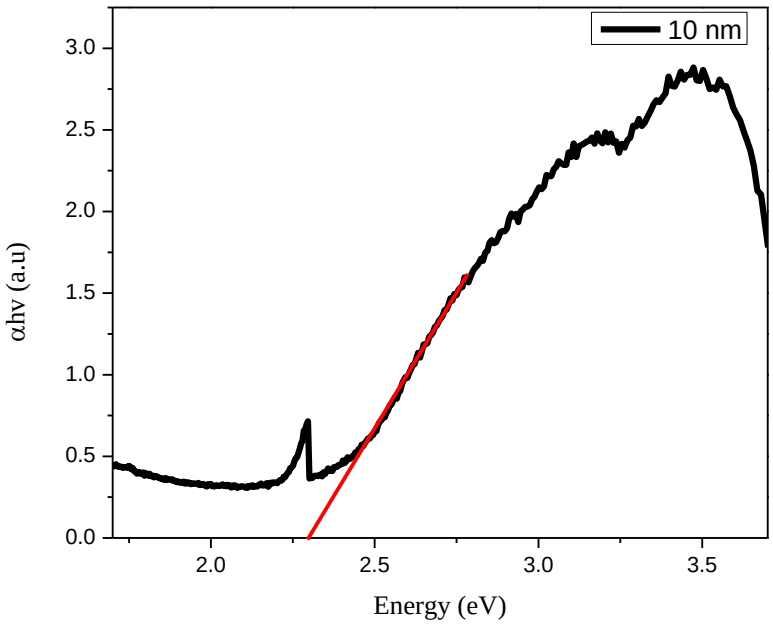

Figure 4.18: Tauc plot of Au10

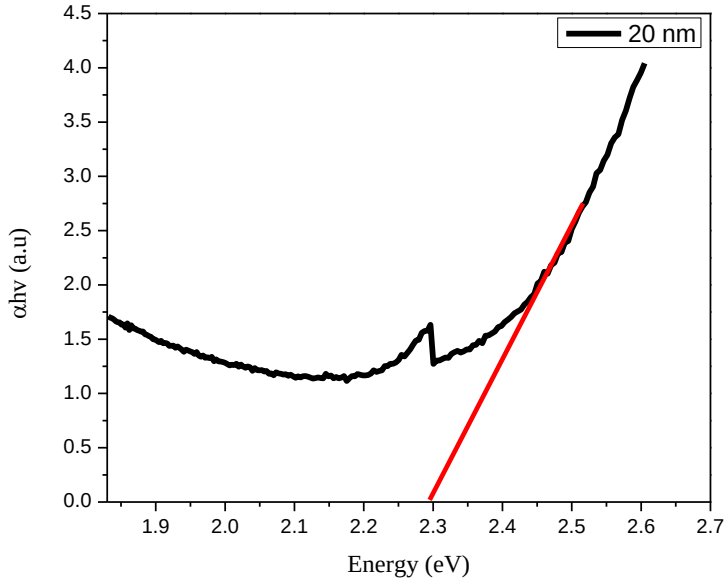

Figure 4.19: Tauc plot of Au20

4.6 Summary

In this chapter, the formation of composite films and their optical and morphological properties are discussed concluding the following final analysis.

- Raman spectroscopy shows the Anatase phase of TiO_2.
- Spectroscopy Ellipsometry measured the thicknesses of the deposited films.
- AFM analysis shows that deposited films were relatively smooth which was an important aspect of deposition to ultimately affect the optical properties of TiO_2.
- Photoluminescence shows 3 luminescent states present in composite films. A shift in the band gap of composite films compared to simple TiO_2 deposition was clearly visible which was also further probed with UV/Vis characterization.
- UV/Vis shows absorption in the visible region for composite films compared to TiO_2 which decreased with the increase in thickness of the Au layer. It also showed a shift of surface plasmon modes towards smaller wavelength with the increase in Au layer. Tauc plots of all 5 samples with different Au thicknesses reveal modification in optical properties of TiO_2.

Conclusion and Future work

The research work presented in this thesis focuses on the deposition of $TiO_2/Au/TiO_2$ composite films and the effect of the thickness of Au layer on the optical properties of TiO_2. Because of its diverse optical, electrical, and magnetic capabilities, gold is used. Gold nanoparticles absorb light in the visible range and can change the optical characteristics of colloidal particles by modifying their size.

In the present thesis, $TiO_2/Au/TiO_2$ composite films are prepared by chemical vapor deposition on silicon (100) substrates. The surface morphology of these composite films was studied using AFM which revealed a smoother deposition of layers which was an important aspect of the experiment.

Raman spectroscopy revealed the presence of E1g, B1g, A1g, and Eg3 vibrational modes and a well-resolved mode at 139.6 cm^{-1} showing the Anatase phase of TiO_2.

Ellipsometry was employed to calculate the accurate thickness of $TiO_2/Au/TiO_2$ layers to study the effect of Au thickness on the optical properties of TiO_2.

Photoluminescence spectroscopy revealed 3 types of luminescent centers in TiO_2 around 351nm, 520nm and in the IR range. PL also revealed the introduction of near band gap edge defects as well as a rounded peak in composite films.

UV/Vis spectroscopy revealed enhanced absorption in the visible region for composite films compared to simple absorption spectrum for TiO_2 only. 1nm thickness showed a drastic amount of absorption intensity compared to any other thickness. With the increase in the thickness of gold, this absorption intensity can be observed to be decreasing. In composite films with thickness of Au to be 5nm, 10nm and 20nm surface plasmon resonance modes are observed around 730nm, 670nm and 620nm respectively showing a shift in SPR modes towards smaller wavelength.

The absorption of Au-embedded TiO_2 films in the visible part of the electromagnetic spectra is quite high. Therefore, their use as cathode material can substantially increase

the incident photon to charge carrier transport efficiency (IPCE) in third-generation solar cells.

Spectroscopic ellipsometry was measured at a single angle. Angle-dependent measurements of Au-embedded TiO_2 thin films should also be carried out to see the polarization effects caused by surface plasmon resonances more clearly.

Furthermore, optical characteristics such as absorption, reflection, transmission, complex refractive and dielectric functions, and many others can be determined using spectroscopic ellipsometry.

Because the absorption and luminescence properties of Au-embedded, Au-coated nanostructures have been greatly enhanced, they should be used in a variety of device applications, such as solar cells, electroluminescent devices, and light emitting devices.

References

[1] https://nanoyou.eu/attachments/188_Module-1-chapter-1.pdf

[2] https://www.nano.gov/nanotech-101/what/definition

[3] https://www.iberdrola.com/innovation/nanotechnology-applications.

[4] https://www.eia.gov/energyexplained/what-is-energy/sources-of-energy.php).

[5] https://www.allthescience.org/what-are-the-different-generations-of-solar-cells.html

[6] Conibeer, G. (2007). Third-generation photovoltaics. Materials today, 10(11), 42-50.

[7] Lansåker, P. (2012). Gold-Based Nanoparticles and Thin Films: Applications to Green Nanotechnology (Doctoral dissertation, Acta Universitatis Upsaliensis).

[8] Kelly, K. L., Coronado, E., Zhao, L. L., & Schatz, G. C. (2003). The optical properties of metal nanoparticles: the influence of size, shape, and dielectric environment. The Journal of Physical Chemistry B, 107(3), 668-677.

[9] Lin, Z., Wang, X., Liu, J., Tian, Z., Dai, L., He, B., ... & Hu, Z. (2015). On the role of localized surface plasmon resonance in UV-Vis light irradiated Au/TiO 2 photocatalysis systems: Pros and cons. Nanoscale, 7(9), 4114-4123.

[10] https://pubchem.ncbi.nlm.nih.gov/compound/Titanium-dioxide#section=SpringerNature-References.

[11] Haider, A. J., Jameel, Z. N., & Taha, S. Y. (2015). Synthesis and characterization of TiO2 nanoparticles via sol-gel method by pulse laser ablation. Eng. & Tech. Journal, 33(5), 761-771.

[12] https://www.lgt.tw/nano-powder-product/145-titanium-dioxide-2-universal-pigment

[13] Noman, M. T., Ashraf, M. A., & Ali, A. (2019). Synthesis and applications of nano-TiO2: a review. Environmental Science and Pollution Research, 26(4), 3262-3291.

[14] Chen, X., & Mao, S. S. (2007). Titanium dioxide nanomaterials: synthesis, properties, modifications, and applications. Chemical reviews, 107(7), 2891-2959.

[15] Gupta, S. M., & Tripathi, M. (2011). A review of TiO2 nanoparticles. chinese science bulletin, 56(16), 1639-1657.

[16] Chen, X., & Mao, S. S. (2007). Titanium dioxide nanomaterials: synthesis, properties, modifications, and applications. Chemical reviews, 107(7), 2891-2959.

[17] Ziental, D., Czarczynska-Goslinska, B., Mlynarczyk, D. T., Glowacka-Sobotta, A., Stanisz, B., Goslinski, T., & Sobotta, L. (2020). Titanium dioxide nanoparticles: prospects and applications in medicine. Nanomaterials, 10(2), 387.

[18] http://tdma.info/what-is-titanium-dioxide/

[19] https://www.surfacenet.de/titanium-dioxide.htm

[20] https://www.azom.com/properties.aspx?ArticleID=1179

[21] Gao, T., & Jelle, B. P. (2013). Thermal conductivity of TiO2 nanotubes. The Journal of Physical Chemistry C, 117(3), 1401-1408.

[22] https://refractiveindex.info/?shelf=main&book=TiO_2&page=Devore-o

[23] Noman, M. T., Ashraf, M. A., & Ali, A. (2019). Synthesis and applications of nano-TiO2: a review. Environmental Science and Pollution Research, 26(4), 3262-3291.

[24] Chen, X., & Mao, S. S. (2007). Titanium dioxide nanomaterials: synthesis, properties, modifications, and applications. Chemical reviews, 107(7), 2891-2959.

[25] Samat, M. H., Ali, A. M. M., Taib, M. F. M., Hassan, O. H., & Yahya, M. Z. A. (2016). Hubbard U calculations on optical properties of 3d transition metal oxide TiO2. Results in physics, 6, 891-896.

[26] Padmanabhan, M., & Prince, P. S. M. (2006). Preventive effect of S-allylcysteine on lipid peroxides and antioxidants in normal and isoproterenol-induced cardiotoxicity in rats: a histopathological study. Toxicology, 224(1-2), 128-137.

[27] Sayes, C. M., Wahi, R., Kurian, P. A., Liu, Y., West, J. L., Ausman, K. D., ... & Colvin, V. L. (2006). Correlating nanoscale titania structure with toxicity: a cytotoxicity and inflammatory response study with human dermal fibroblasts and human lung epithelial cells. Toxicological sciences, 92(1), 174-185.

[28] Xue, C., Wu, J., Lan, F., Liu, W., Yang, X., Zeng, F., & Xu, H. (2010). Nano titanium dioxide induces the generation of ROS and potential damage in HaCaT cells under UVA irradiation. Journal of nanoscience and nanotechnology, 10(12), 8500-8507.

[29] Petković, J., Žegura, B., Stevanović, M., Drnovšek, N., Uskoković, D., Novak, S., & Filipič, M. (2011). DNA damage and alterations in expression of DNA damage responsive genes induced by TiO2 nanoparticles in human hepatoma HepG2 cells. Nanotoxicology, 5(3), 341-353.

[30] Andersson, P. O., Lejon, C., Ekstrand-Hammarström, B., Akfur, C., Ahlinder, L., Bucht, A., & Österlund, L. (2011). Polymorph-and size-dependent uptake and toxicity of TiO2 nanoparticles in living lung epithelial cells. Small, 7(4), 514-523.

[31] Shi, H., Magaye, R., Castranova, V., & Zhao, J. (2013). Titanium dioxide nanoparticles: a review of current toxicological data. Particle and fibre toxicology, 10(1), 1-33.

[32] Pawlowski, L., & Blanchart, P. (2018). Industrial chemistry of oxides for emerging applications. John Wiley & Sons.

[33] Haider, A. J., Jameel, Z. N., & Al-Hussaini, I. H. (2019). Review on: titanium dioxide applications. Energy Procedia, 157, 17-29.

[34] Park, M. C., Yoon, W. H., Lee, D. H., Myoung, J. M., Bae, S. H., Lee, S. Y., & Yun, I. (2001). Effects of misfit strain on properties of ZnO films grown by pulsed laser deposition. MRS Online Proceedings Library (OPL), 696.

[35] Freeman, R. G., Grabar, K. C., Allison, K. J., Bright, R. M., Davis, J. A., Guthrie, A. P., ... & Natan, M. J. (1995). Self-assembled metal colloid monolayers: an approach to SERS substrates. Science, 267(5204), 1629-1632.

[36] Taton, T. A., Mirkin, C. A., & Letsinger, R. L. (2000). Scanometric DNA array detection with nanoparticle probes. science, 289(5485), 1757-1760.

[37] Nath, N., & Chilkoti, A. (2002). A colorimetric gold nanoparticle sensor to interrogate biomolecular interactions in real time on a surface. Analytical chemistry, 74(3), 504-509.

[38] Das, M., Shim, K. H., An, S. S. A., & Yi, D. K. (2011). Review on gold nanoparticles and their applications. Toxicology and Environmental Health Sciences, 3(4), 193-205.

[39] Yeh, Y. C., Creran, B., & Rotello, V. M. (2012). Gold nanoparticles: preparation, properties, and applications in bionanotechnology. Nanoscale, 4(6), 1871-1880.

[40] Amendola, V., Meneghetti, M., Stener, M., Guo, Y., Chen, S., Crespo, P., ... & Pasquato, L. (2014). Physico-chemical characteristics of gold nanoparticles. In Comprehensive analytical chemistry (Vol. 66, pp. 81-152). Elsevier.

[41] www.sigmaaldrich.com/technical-Documents/articles/materialsscience/nanomaterials/gold-nanoparticles.html.

[42] www.iue.tuwien.ac.at/phd/filipovic/node26.html.

[43] Fan, Z., Huang, X., Tan, C., & Zhang, H. (2015). Thin metal nanostructures: synthesis, properties and applications. Chemical Science, 6(1), 95-111.

[44] Ahmed, S., & Ikram, S. (2016). Biosynthesis of gold nanoparticles: a green approach. Journal of Photochemistry and Photobiology B: Biology, 161, 141-153.

[45] Yeh, Y. C., Creran, B., & Rotello, V. M. (2012). Gold nanoparticles: preparation, properties, and applications in bionanotechnology. Nanoscale, 4(6), 1871-1880.

[46] Haugstad, G. (2012). Atomic force microscopy: understanding basic modes and advanced applications. John Wiley & Sons.

[47] www.researchgate.net/figure/Fig-1-Working-modes-of-AFM-a-contact-mode-b-non-contact-mode-c-tapping-mode_fig1_233692544.

[48] Balachandran, U. G. E. N., & Eror, N. G. (1982). Raman spectra of titanium dioxide. Journal of Solid State Chemistry, 42(3), 276-282.

[49] Javed, F., Javed, S., Mujahid, M., ul Inam, F., & Bhatti, A. S. (2019). Modified optical characteristics of TiO2/Au/TiO2 thin composite films. Ceramics International, 45(17), 22336-22343.